Dislocation modeling of blind thrusts in the eastern Los Angeles basin, California

Daniel J. Myers
Division of Natural Sciences and Mathematics, Western Oregon University, Monmouth, Oregon, USA

John L. Nabelek
College of Oceanic and Atmospheric Sciences, Oregon State University, Corvallis, Oregon, USA

Robert S. Yeats
Department of Geosciences, Oregon State University, Corvallis, Oregon, USA

Received 9 August 2002; revised 25 April 2003; accepted 18 June 2003; published 25 September 2003.

[1] The East and West Coyote Hills in the eastern Los Angeles Basin are the surface expression of uplift accompanying blind reverse faulting. Folded Quaternary strata indicate that the hills are growing and that the faults underlying them are active. Detailed subsurface mapping in the East Coyote Oil Field shows that a previously mapped, reverse separation fault is predominantly an inactive, left-lateral, strike-slip fault that is not responsible for the uplift of the East Coyote Hills. The fault responsible for folding and uplift of the Coyote Hills does not cut wells in either the East or West Coyote Oil Fields. To characterize the geometry of the blind fault responsible for folding, we employ dislocation modeling. The dip and upper fault tip depths obtained from modeling suggest that the thrust fault beneath the Coyote Hills may be an extension of the Puente Hills blind thrust fault that continues westward beneath the Santa Fe Springs Oil Field. Modeling results suggest that the segment of the thrust fault responsible for folding the Coyote Hills would have accumulated 1500 m of reverse displacement over the last 1.2 Myr, yielding an average slip rate of 1.3 ± 0.5 mm/yr. The Santa Fe Springs segment of the fault has a slip rate of 1.5 ± 0.4 mm/yr for the last 1.2 Myr. The estimated moment magnitude for a reverse displacement earthquake on the Puente Hills blind thrust ranges from 6.6 to 7.2, depending on the length of the rupture. The estimated average recurrence interval for these earthquakes is 1700–3200 years. *INDEX TERMS:* 7260 Seismology: Theory and modeling; 8005 Structural Geology: Folds and folding; 8010 Structural Geology: Fractures and faults; 8015 Structural Geology: Local crustal structure; 8107 Tectonophysics: Continental neotectonics; *KEYWORDS:* blind thrust faults, southern California, earthquakes

Citation: Myers, D. J., J. L. Nabelek, and R. S. Yeats, Dislocation modeling of blind thrusts in the eastern Los Angeles basin, California, *J. Geophys. Res.*, *108*(B9), 2443, doi:10.1029/2002JB002150, 2003.

1. Introduction

[2] In recent years, following the 1987 Whittier Narrows (*M* 5.9) and 1994 Northridge (*M* 6.7) earthquakes, research in the Los Angeles metropolitan area has focused on identifying and characterizing the earthquake hazard from blind thrusts. This task is difficult because the faults do not reach the surface, and they must be studied by analysis of the overlying folds that accompany fault displacement at depth. Active folding in the Los Angeles Basin is accompanied by uplift, so that the presence of hilly topography within the basin is evidence for an active tectonic history. Furthermore, because the Los Angeles Basin is an oil-producing area, well logs and multichannel seismic profiles permit three-dimensional analysis of fold structure, commonly in great detail.

[3] The Whittier Narrows earthquake ruptured a segment of a blind thrust that extends from downtown Los Angeles eastward to the Santa Ana River; this thrust, now expressed as actively growing anticlines (Figure 1a), had not been recognized as a seismic hazard prior to the earthquake [*Davis et al.*, 1989; *Shaw and Suppe*, 1996]. *Shaw and Shearer* [1999] named this feature the Puente Hills thrust. They were able to map the 1987 fault in the subsurface based on the distribution of relocated main shock and aftershock earthquakes and on fault plane reflections from industry seismic profiles beneath the Santa Fe Springs Oil Field, which is enclosed by the Santa Fe Springs anticline on Figures 1a and 1b. Modeling of this structure, using the trishear method, was done by *Allmendinger and Shaw* [2000].

[4] The Coyote Hills anticlines localize the West Coyote (WC) and East Coyote (EC) oil fields. We use dislocation

0148-0227/03/2002JB002150$09.00

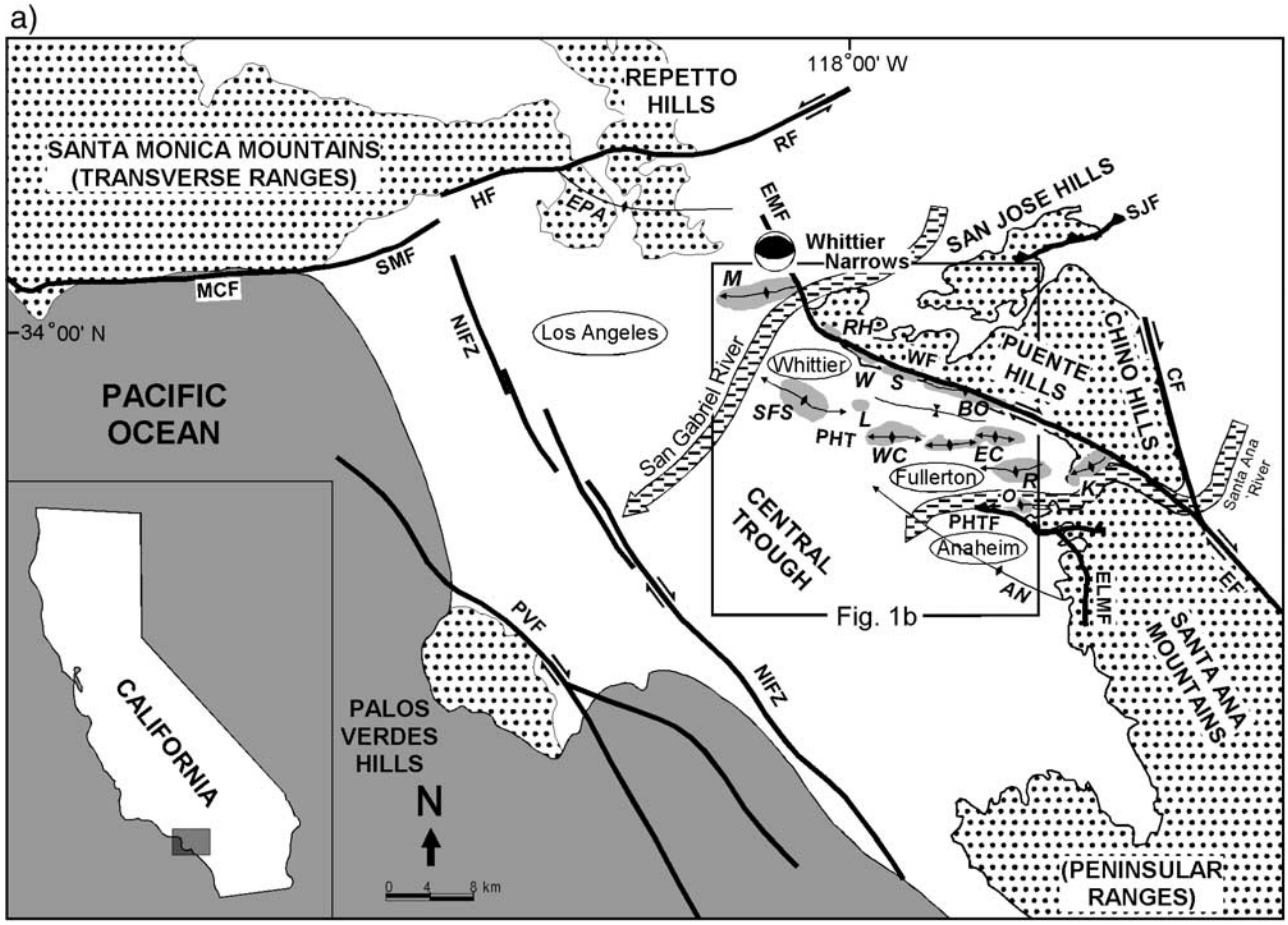
a)
118°00' W
REPETTO HILLS
SANTA MONICA MOUNTAINS (TRANSVERSE RANGES)
RF
HF
EPA
EMF
SAN JOSE HILLS
SJF
Whittier Narrows
SMF
MCF
34°00' N
M
RH
WF
W
S
BO
SFS
L
PHT
WC
EC
R
O
K?
PHTF
Anaheim
AN
ELMF
EF
CF
CHINO HILLS
PUENTE HILLS
Santa Ana River
San Gabriel River
Los Angeles
NIFZ
PACIFIC OCEAN
CENTRAL TROUGH
Fig. 1b
PVF
PALOS VERDES HILLS
CALIFORNIA
N
0 4 8 km
SANTA ANA MOUNTAINS
(PENINSULAR RANGES)

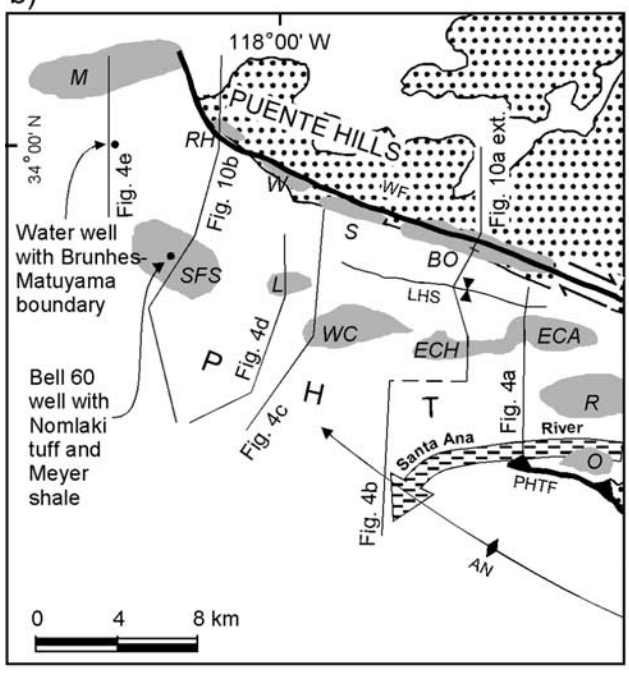
b)
118°00' W
34°00' N
M
RH
PUENTE HILLS
W
WF
S
BO
SFS
L
LHS
WC
ECH
ECA
R
O
PHTF
AN
Fig. 4e
Fig. 10b
Fig. 10a ext.
Fig. 4d
Fig. 4c
Fig. 4a
Fig. 4b
Water well with Brunhes-Matuyama boundary
Bell 60 well with Nomlaki tuff and Meyer shale
Santa Ana River
0 4 8 km

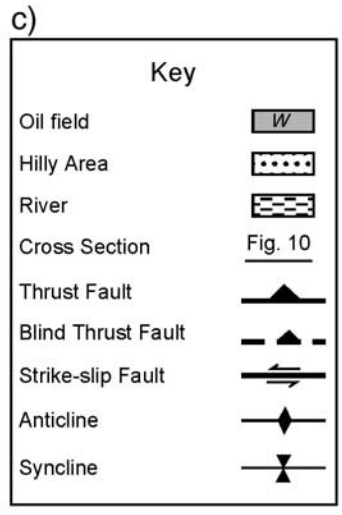
c)
Key
Oil field
W
Hilly Area
River
Cross Section
Fig. 10
Thrust Fault
Blind Thrust Fault
Strike-slip Fault
Anticline
Syncline

modeling of the Coyote Hills anticline at East Coyote, where an unusually complete subsurface data set is available to resolve the structural history and fold configuration, to determine the location and slip rate on the blind thrust beneath the Coyote Hills anticline. We then apply the dislocation modeling method to the Santa Fe Springs anticline immediately to the west, where the 1987 Whittier Narrows blind thrust has been located from seismicity and fault plane reflections [*Shaw and Shearer*, 1999]. Finally, we consider the implications of the convergence rate across this blind structure on the distribution of shortening across the Los Angeles Basin as measured by Global Positioning System (GPS) data [*Bawden et al.*, 2001], and the partitioning of slip on the Elsinore fault among the Whittier and Chino surface faults and the Puente Hills blind thrust.

2. Tectonic Setting

[5] The Los Angeles Basin is within the transition zone between the west trending Transverse Ranges on the north and the northwest trending Peninsular Ranges on the south (Figure 1a). Internal structures in the basin, including the Newport-Inglewood fault zone, the Central Trough, the Anaheim nose, and the Whittier fault, have a Peninsular Ranges trend. However, a set of anticlines within the northeast part of the basin trend east-west, parallel to the Transverse Ranges. The focal mechanism of the Whittier Narrows earthquake also revealed an east-west striking fault plane [*Bent and Helmberger*, 1989; *Hauksson and Jones*, 1989], an echo of the Transverse Ranges to the north. The folds, all sites of oil fields [*Wright*, 1991], are from west to east, the Santa Fe Springs, West Coyote, East Coyote-Hualde, East Coyote-Anaheim, Richfield, and Kraemer anticlines. On the west, the Santa Fe Springs anticline either terminates westward near the San Gabriel River or is stepped to the right to the Elysian Park anticline in downtown Los Angeles [*Oskin et al.*, 2000]. A right step over also marks the boundary between the Santa Fe Springs and West Coyote anticlines. On the east, the Richfield and Kraemer anticlines intersect the west-northwest trending, right-lateral, strike-slip Whittier fault near the Santa Ana River (Figure 1a).

[6] The Whittier fault lies near the southern range front of the Puente Hills, which are themselves uplifted along a southward vergent anticline. The La Habra syncline (LHS, Figure 1b), located between the Puente Hills and the Coyote Hills, appears to be active based on syntectonic thickening of late Quaternary strata. South of the Coyote Hills, the northwest trending subsurface Anaheim nose (AN, Figure 1b) bounds the northeastern side of the Central Trough of the Los Angeles basin. Although the Anaheim nose contains deformed strata as young as Pliocene, overlying Quaternary strata do not appear to be deformed, based on oil-industry seismic reflection profiles.

3. Stratigraphy

[7] The northeastern Los Angeles Basin is underlain by a sequence of Late Cretaceous through early Miocene sedimentary strata that are correlated to surface exposures in the Santa Ana Mountains to the east. These strata, deposited prior to the formation of the Los Angeles Basin as a separate tectonic feature, contain no information about basin evolution. This sequence is overlain by marine sandstone, siltstone, and shale of the middle Miocene Topanga Group, the upper Miocene Puente Formation, and the Pliocene Repetto Member of the Fernando Formation [*Barron and Isaacs*, 2001; *Blake*, 1991]. ''Delmontian'' strata, the youngest part of the Puente Formation, lens out to the west so that in wells in the westernmost part of the East Coyote Oil Field, lower Repetto rests directly on Mohnian strata (Figure 2 and Appendix A). Sandstone and shale of the lower/middle part of the Repetto Member are divided into the Third Anaheim, Second Anaheim, and First Anaheim oil-producing zones. The contact between the Repetto and Pico members of the Fernando Formation is commonly marked by a transition from silty, shaly, relatively sandstone-free strata of the upper Repetto to the sandier siltstone of the Pico, which contains numerous discontinuous sandstone beds.

[8] Quaternary strata overlying the Pico Member include, in ascending order, the San Pedro, Coyote Hills, and La Habra Formations, as well as alluvial and colluvial deposits [*Yerkes*, 1972; *Tan et al.*, 1984]. The La Habra Formation overlies the Coyote Hills Formation along a low-angle unconformity. Of the Quaternary stratigraphic units, only the Pico-San Pedro contact is mapped in the subsurface. The top of the Coyote Hills Formation could not be mapped, in large part because these contacts could not be logged in most wells. Additional stratigraphic detail and a type electric log are provided in Appendix A.

4. Structure

[9] The Coyote Hills are underlain by a series of doubly plunging, en echelon anticlines, or domes, trending east-west. The West Coyote dome is stepped right with respect to the Hualde dome, which is itself stepped left with respect to the Anaheim dome (Figure 1b). Despite the east-west trend

Figure 1. (opposite) (a) Location of oil fields (shaded) in anticlines overlying blind thrusts in the northeastern Los Angeles Basin. Fault abbreviations: CF, Chino fault; EF, Elsinore fault; ELMF, El Modeno fault; EMF, East Montebello fault; HF, Hollywood fault; MCF, Malibu Coast fault; NIFZ, Newport-Inglewood fault zone; PHTF, Peralta Hills thrust fault; PHT, Puente Hills blind thrust; PVF, Palos Verdes fault; RF, Raymond fault; SJF, San Jose fault; SMF, Santa Monica fault; WF, Whittier fault. Oil field abbreviations: BO, Brea-Olinda; EC, East Coyote; K, Kraemer; L, Leffingwell; M, Montebello; O, Olive; R, Richfield; RH, Rideout Heights; S, Sansinena; SFS, Santa Fe Springs; W, Whittier; WC, West Coyote. Other structures: AN, Anaheim Nose; EPA, Elysian Park anticline. Ellipses contain city names. Focal mechanism shown for 1987 Whittier Narrows earthquake [*Hauksson and Jones*, 1989]. Data from *Gray* [1961], *Yerkes et al.* [1965], and *Wright* [1991]. (b) Location of cross sections, Brunhes-Matuyama magnetic chron boundary, and dated Nomlaki tuff; abbreviations same as Figure 1a except ECA, Anaheim dome of East Coyote Oil Field; ECH, Hualde dome of East Coyote Oil Field; LHS, La Habra syncline.

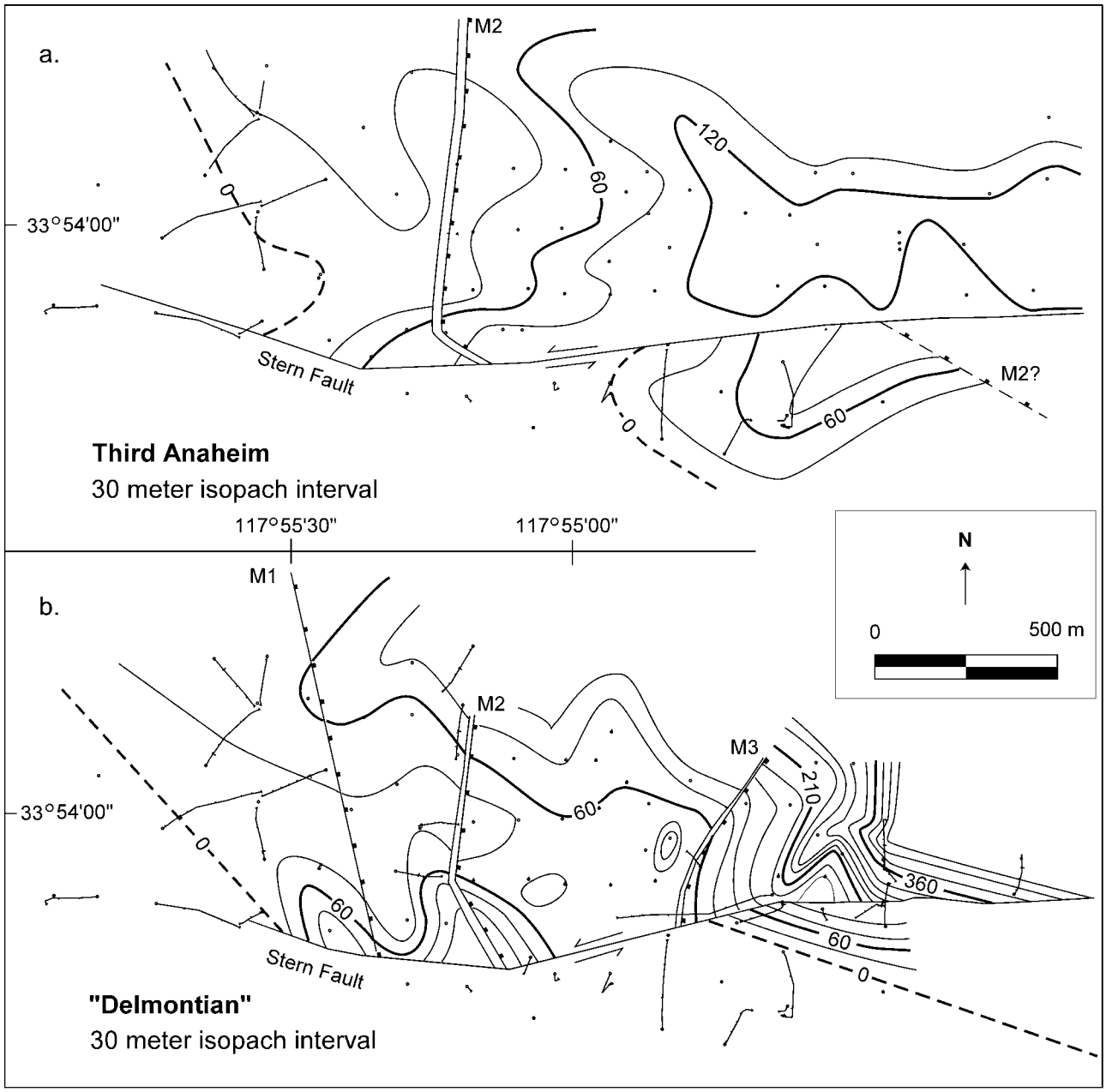

Figure 2. Isopachs of (a) Third Anaheim zone and (b) "Delmontian" strata in the Hualde dome of East Coyote Oil Field. Pinchouts in both units are consistent with approximately 1200 m of left-lateral offset on the Stern fault. Dots show well control, with lines extending from dots the map projection of directionally drilled wells. M1, M2, and M3 identify Miocene normal faults. Black squares are on the down-thrown, hanging wall sides of faults. Faults have been shown by a double line where both faults and horizon have been structurally contoured; see *Tearpock and Bischke* [1991] for an explanation of techniques. For well names and detailed well locations, see maps W1-5 and 102–106 of *California Division of Oil, Gas, and Geothermal Resources* [2000, 1997a, 1997b, 1997c, 1997d, 1997e]. Map projection of directional well courses are based on well surveys from the Unocal Corporation.

of the dome, the hills overlying the Hualde dome trend northeast-southwest as a result of the southwest orientation of Fullerton and Brea creeks (Figure 3). The topography indicates that the southwest flowing drainage was in place prior to uplift of the domes. The drainage pattern developed at the end of the depositional stage, after the deposition of the nonmarine Coyote Hills and La Habra formations. Subsequent growth was accompanied by uplift, incising the drainage into the rising Coyote Hills.

[10] At first glance, the Coyote Hills anticlines appear to be the result of reverse displacement on the South Flank fault of West Coyote and the Stern fault of East Coyote

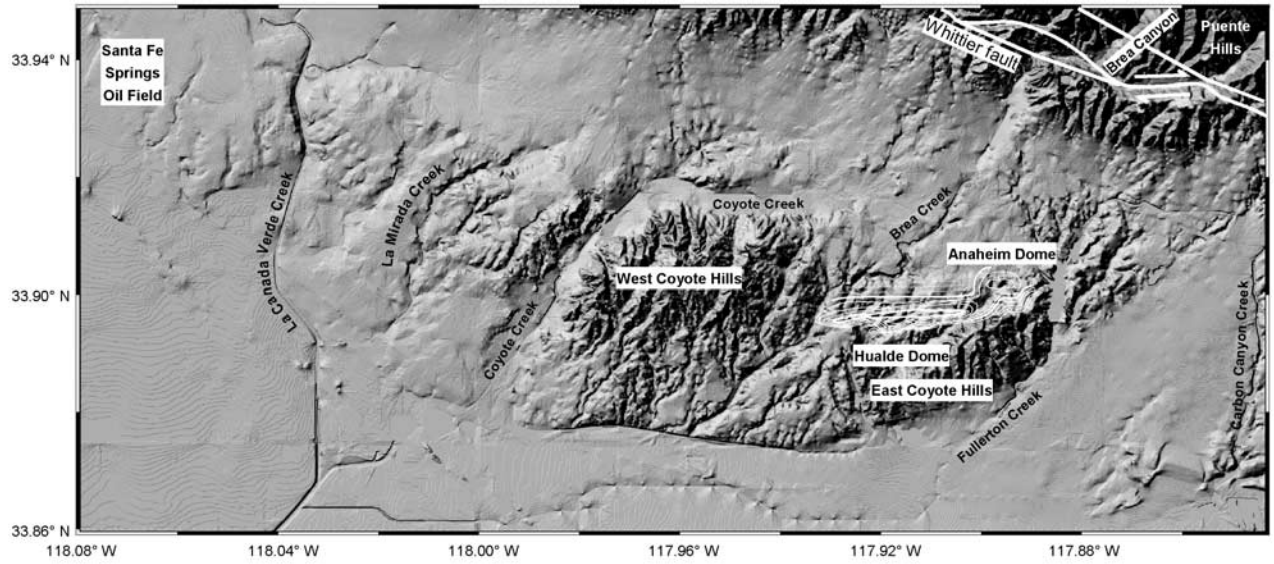

Figure 3. Digital elevation model of the Coyote Hills, together with structure contours on the base of the San Pedro Formation in the East Coyote Oil Field. The east trend of the structure contours of Hualde dome is in contrast to the northeast-southwest trend of the topography due to the southwest direction of the drainage of Fullerton Creek and Brea Creek. Establishment of drainage predated uplift. The scarp at the south edge of the hills between longitude 117.92°W and 117.99°W is a fold scarp possibly related to the blind Puente Hills thrust beneath the Coyote Hills [cf. *Williams et al.*, 2000]. The structure contour interval is 50 m, with the innermost contour value being 90 m below sea level. The next heavy contour line is the 240 m contour. Trace of Whittier fault from *Dibblee* [2001a, 2001b].

(Figures 4a–4c. These faults strike parallel to the Coyote anticlines along their southern flanks [*Yerkes*, 1972; *Wright*, 1991]. Fault structure contours, however, show that these are the same fault (Figure 5). Structure contours of the South Flank fault have been continued west of the Coyote Hills anticline to the area between the Leffingwell Oil Field and La Mirada Oil Field on the Anaheim nose (Figures 4d and 5). The Stern fault has not been found in the Anaheim dome (Figure 4a). An eastward projection of the fault would lie south of the anticline (Figure 5) in an area with no well control. We conclude that the fault passes between wells C and D in Figure 4a. The differing spatial relationship between the Stern fault and the Hualde and Anaheim domes suggests that the Stern fault is not responsible for the growth of these structures.

[11] Offset structures and stratigraphy demonstrate that the sense of motion along the South Flank-Stern fault is predominantly left-lateral strike slip, not reverse slip. The fault offsets three east dipping normal faults in the Hualde dome of the East Coyote Oil field (M1, M2, and M3 in Figure 2). These normal faults appear to be mainly late Miocene in age, although the M2 fault cuts strata as young as the base of the First Anaheim zone in the Repetto Formation [*Myers*, 2001]. The Stern fault also offsets isopachs and the zero pinchout lines of the ''Delmontian'' and Third Anaheim zones, which are displaced left laterally 1100 ± 200 m (Figure 2). Further evidence that the fault is strike slip includes the normal dip separation of Miocene strata in the Hualde dome, in contrast to the reverse dip separation in Repetto strata (Figure 4b), and abrupt stratigraphic thickness changes across the South Flank-Stern fault (Figures 2, 4b, and 4c).

[12] The timing of displacement along the South Flank-Stern fault and the initiation of folding also argue that the Coyote folds and the faults are unrelated (Figure 4). The Pico and upper Repetto members show thinning across the crest of the Hualde dome, whereas the middle and lower Repetto members show no thinning, indicating that the folds began to grow during the deposition of the upper Repetto. Similar syndepositional growth in the Los Angeles Basin was documented by *Shaw and Suppe* [1996] and *Schneider et al.* [1996]. Strike-slip displacement along the South Flank-Stern fault would have occurred earlier, largely during deposition of the Repetto and ended during deposition of the Pico member of the Fernando Formation.

[13] The change in dip with increasing depth and the timing of offset along the South Flank-Stern fault demonstrate that the fault is folded along with the strata (Figures 4b and 5), consistent with the South Flank-Stern fault predating the folding of the Coyote anticlines. When the post-Pico folding is removed, the north dipping South Flank-Stern fault changes to nearly vertical or steeply south dipping (Figures 4b–4d), which is consistent with strike slip rather than dip slip on the South Flank-Stern fault. We conclude that the South Flank-Stern fault is not responsible for the growth of the Coyote Hills and that the fault responsible for the growth of the anticlines is blind and not cut by any wells.

5. Modeling of the Coyote Hills Fold and Blind Thrust

[14] Because the South Flank-Stern fault is not directly related to the growth of the Coyote folds, it is necessary to

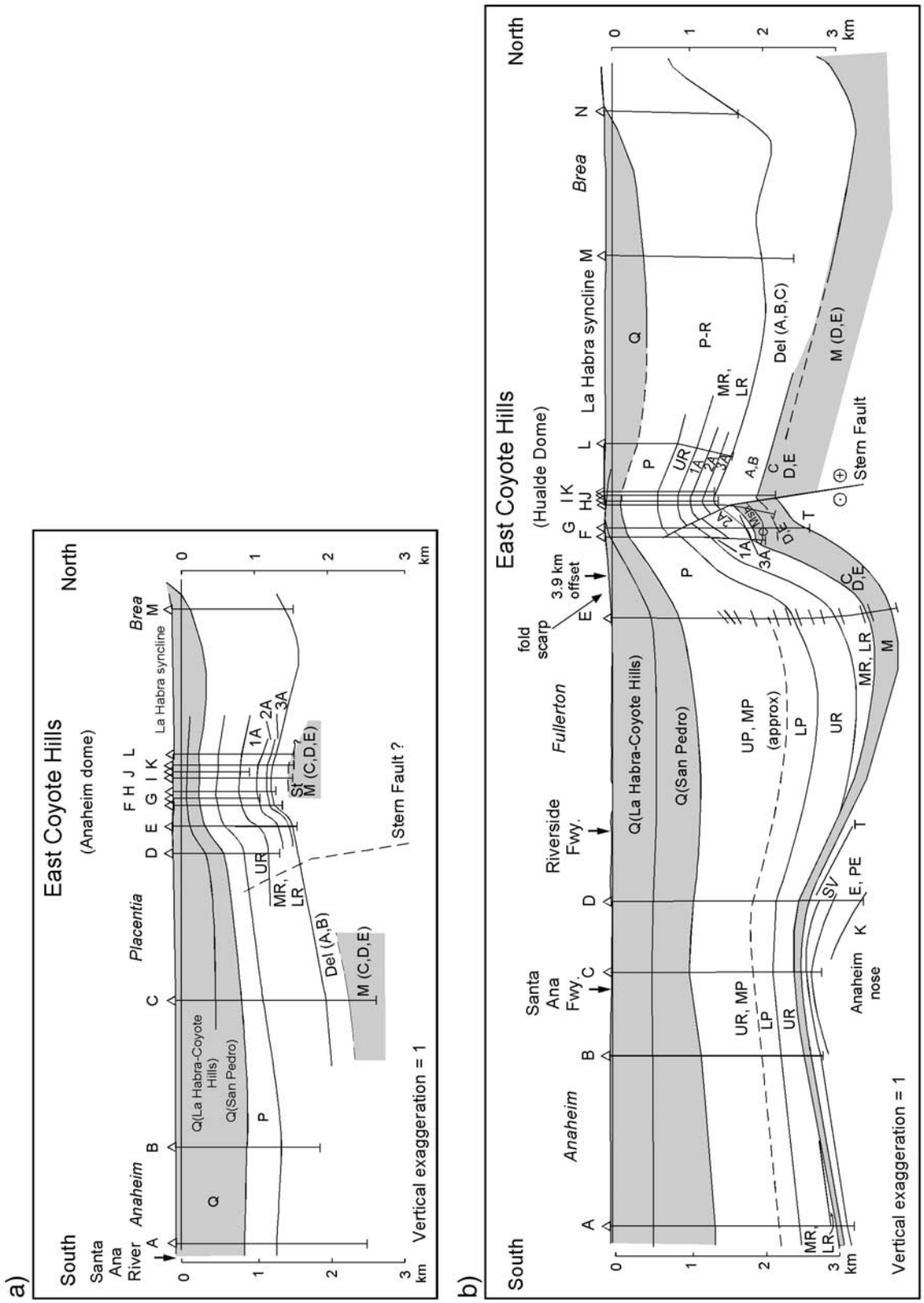
a)
East Coyote Hills
(Anaheim dome)
South
North
Santa Ana River
Anaheim
Placentia
Brea
La Habra syncline
A B C D E F H J K L M
Q
Q(La Habra-Coyote Hills)
Q(San Pedro)
P
UR
MR, LR
1A
2A
3A
M (C,D,E)
Del (A,B)
M (C,D,E)
Stem Fault ?
0 1 2 3 km
Vertical exaggeration = 1
b)
East Coyote Hills
(Hualde Dome)
South
North
Anaheim
Fullerton
Brea
Santa Ana Fwy.
Riverside Fwy.
fold scarp
3.9 km offset
La Habra syncline
A B C D E F G H I J K L M N
Q(La Habra-Coyote Hills)
Q(San Pedro)
Q
P
P-R
UP, MP (approx)
LP
UR
UR, MP
LP
MR, LR
1A
2A
3A
A,B
C
D,E
Del (A,B,C)
M (D,E)
M
SV
E, PE
T
Stem Fault
Anaheim nose
0 1 2 3 km
Vertical exaggeration = 1

constrain the geometry and displacement of the source fault by mechanical or kinematic modeling to reproduce the observed folding. We choose dislocation modeling based on its past success in studying blind reverse faults [*Ward and Valensise*, 1994; *Benedetti et al.*, 2000]. We used the three-dimensional dislocation modeling software of *Toda et al.* [1998] and *King et al.* [1994], which is based on the theoretical formulation of *Okada* [1992]. The dislocation is placed in a homogeneous half-space. The Coyote Hills structure formed over a period longer than a million years, during which time most of the shear stress has been relaxed. Crustal deformation is a visco-elastic process, but the effect of viscous relaxation on the shape of the fold occurs at wavelengths longer than that of the Coyote Hills [*King et al.*, 1988] and so has a small impact on the fold shape (less than 5% for fold amplitude and wavelength).

[15] To simulate complete shear relaxation of the lithosphere, the shear modulus is set to zero following *Ward* [1986]. The modeling software allows variation in Young's modulus and Poisson's ratio. Setting the shear modulus to zero corresponds to a Poisson's ratio of 0.5. Varying Young's modulus has no effect on fold shape because Young's modulus cancels out of the equations for dislocation-induced displacement within the half-space. The effect of assuming relaxed moduli on the shape of the fold is minor.

[16] To identify the fault plane that best reproduces the observed folding of the Coyote Hills anticline requires fitting for seven fault parameters: (1) depth of the upper fault tip, (2) north-south horizontal location of the upper fault tip, (3) the east-west horizontal location of the upper fault tip, (4) depth of the lower fault tip, (5) fault length, (6) fault dip, and (7) fault displacement (Figure 6). The amount of data and the modeling procedure determine the parameters that can realistically be determined (see below).

[17] Relief on the fold is constrained by wells far from the East and West Coyote Oil Fields. Strata at these locations are approximately equidistant from the West Coyote Oil Field, and the Hualde and Anaheim domes of the East Coyote Oil Field and have been affected by deformation of all three structures. To model the deformation completely, it would be necessary to allow variation in the geometry and displacement of three faults independently, one underlying each dome. Subsurface well control on the flanks of the folds is sparse, limiting the usefulness of fitting three separate model folds to the observed folds. We therefore simplify the problem by modeling the folding of the East and West Coyote anticlines using a single fault underlying all three folds, although in reality, the fault might be en echelon. A consequence of this simplifying assumption is that evaluating model fit in three dimensions is unnecessary. Instead, the fit of the three-dimensional model to the observed fold is evaluated by comparing a profile of the model fold taken perpendicular to the trend of the fold across its center to a north-south profile across the crest of one of the Coyote anticlines at a right angle to the trend of the fold. Since the folds at East and West Coyote have similar shapes and relief (Figures 4b and 4c), we fit only the Hualde dome of the East Coyote Oil Field.

[18] Fitting a profile of a three-dimensional dislocation model fold to a profile of the observed fold does not allow unique determination of the best fit fault length and depth to the lower fault tip because varying these two parameters produces similar changes in the model profile (Figure 7). Shallowing the lower fault tip or shortening the fault length both result in reductions of fold amplitude and wavelength that are similar in magnitude. Because subsurface well data place some constraints on the length of the fault from the along-strike extent of folding, we choose to fix that parameter of the model. A fault 14 km long extending from the western edge of West Coyote to the eastern edge of the Anaheim dome of East Coyote is a reasonable estimate of fault length.

[19] Assumption of a 14 km fault length and fitting the model fold to a north-south profile across the crest of the Hualde dome reduces the number of parameters to fit to 5. We take a grid-search approach, considering many possible combinations of dip, north-south horizontal location of upper fault tip, depth to upper fault tip, depth to lower fault tip, and displacement. The model displacement is constant at all locations on the fault plane. In reality, fault displacement decreases toward the upper fault tip, so model estimates of displacement should be viewed as averages over depth. Goodness of model fit to the chosen stratigraphic surface is evaluated using a least squares difference method (χ^2) [*Press et al.*, 1992]. A stacked Hualde dome profile is created by projecting all of the electric log well picks for a deformed stratigraphic surface within the Hualde dome and in wells outside of the East Coyote Oil Field onto a north-south vertical plane (Figure 8). We modeled the deformation of the Pico-San Pedro contact, the stratigraphically highest horizon that could be mapped using electric log data (contours on Figure 3). Results from modeling this surface suggest that deeper stratigraphic surfaces might be cut by the fault responsible for the folding and cannot be used to constrain the fault geometry.

[20] The best fit fault based on modeling the Pico-San Pedro contact has a dip of $25° \, ^{+40°}/_{-10°}$N ($^{+}/_{-}$ indicate acceptable parameter range), reverse displacement of 1500 ± 500 m, an upper fault tip depth of 1.5 ± 0.5 km, a horizontal upper tip location of $1.0 \, ^{+0.4}/_{-0.8}$ km north of well E in

Figure 4. (opposite) North-south cross sections through the Coyote folds, Leffingwell Oil Field, and Montebello Oil Field, located on Figure 1b. Symbols are Q, Quaternary; P, Pico; P-R, Pico-Repetto undifferentiated; UP, MP, LP, upper, middle, and lower Pico; UR, MR, LR, upper, middle, and lower Repetto; 1A, First Anaheim; 2A, Second Anaheim; 3A, Third Anaheim; D, ''Delmontian'' or Sycamore Canyon Member (Tsc) of *Yerkes* [1972]; Msh, Mohnian shale; St, Stern zone; M, Miocene; A, B, C, D, E, biostratigraphic zones of *Wissler* [1958]; T, Topanga Formation; and SV, E, PE, K, older formations. Mohnian and post-Fernando strata are shaded. Short lines on well courses show bedding dip based on cores or dipmeter logs. City names in italics. (a) Anaheim dome, East Coyote Oil Field; (b) Hualde dome, East Coyote Oil Field and Anaheim Nose; (c) West Coyote Oil Field and Anaheim Nose; (d) Leffingwell Oil Field and Anaheim Nose; and (e) Montebello Oil Field. Letters on wells refer to identification in Appendix B (see also Tables B1 to B5).

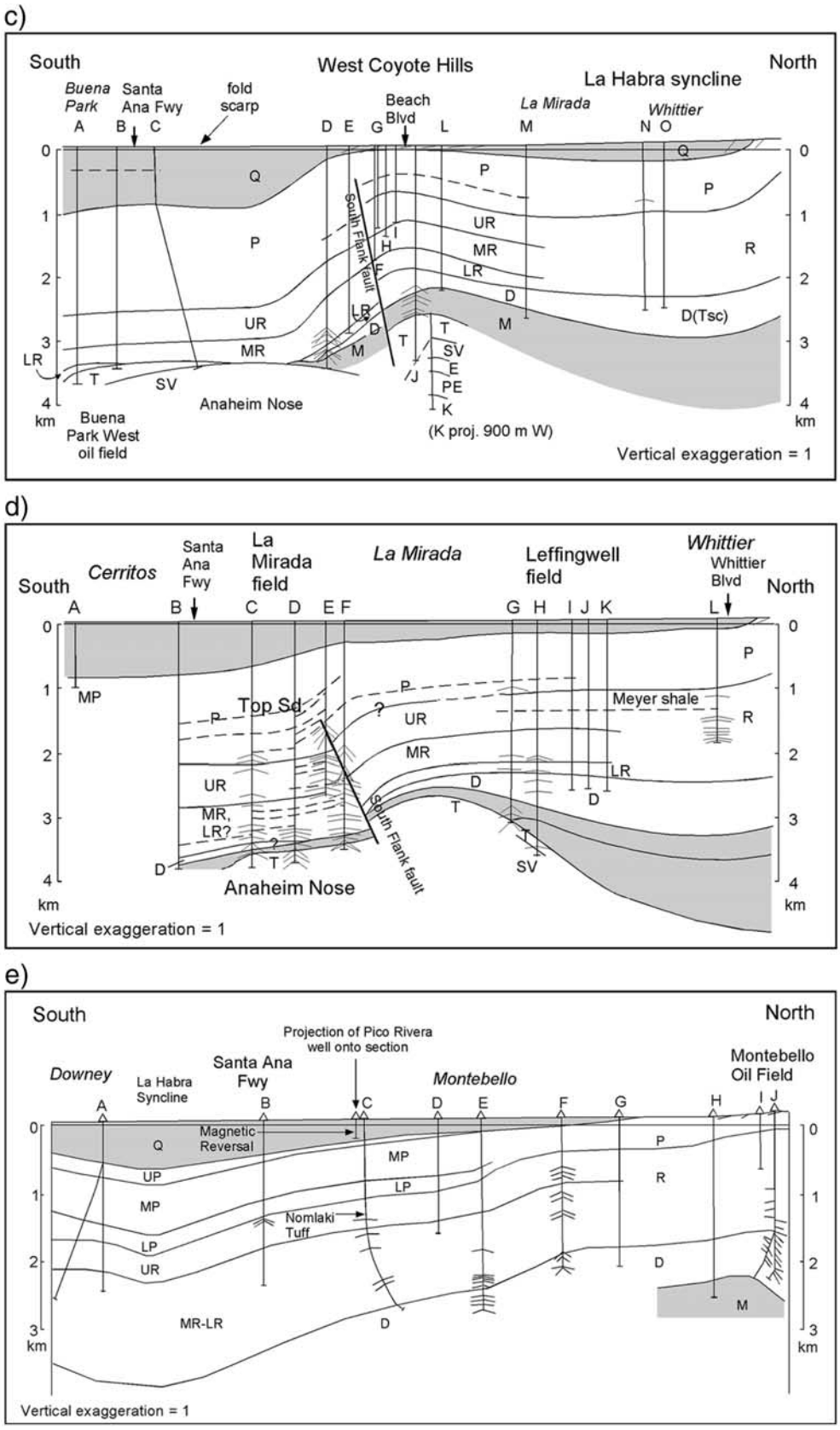

Figure 4. (continued)

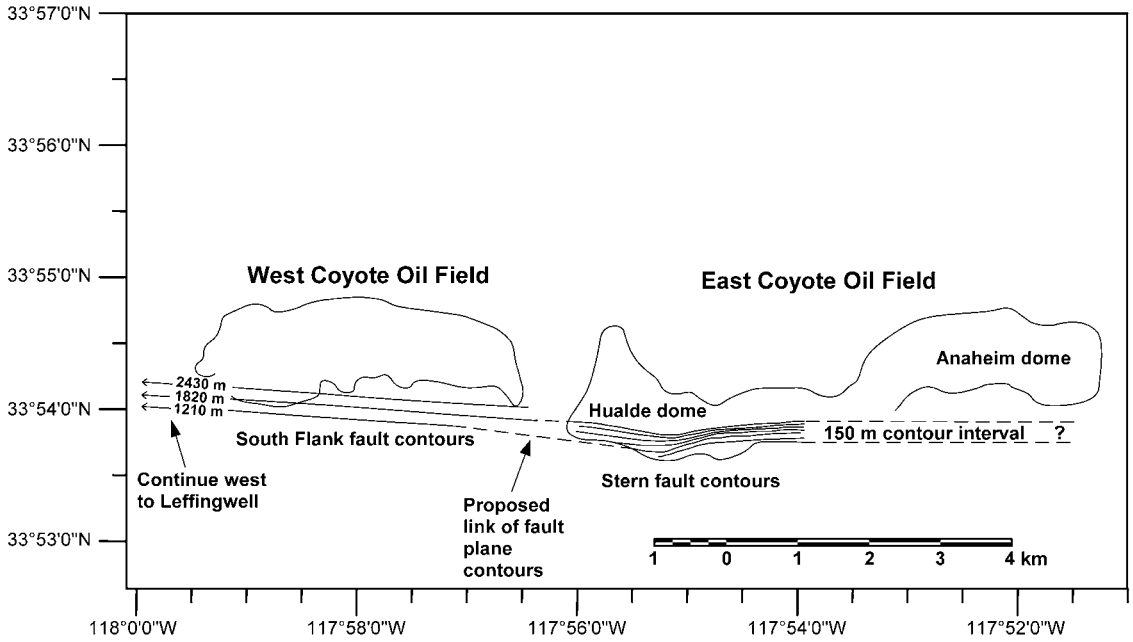

Figure 5. Fault plane contours of the Stern and South Flank faults, showing that the two faults connect between West Coyote and East Coyote. The South Flank fault continues west to an area south of Leffingwell Oil Field (Figure 4d). The Stern fault must continue eastward south of the Anaheim dome of East Coyote Oil Field (Figure 4a). Outlines denote limits of oil fields.

Figure 4b, a lower fault tip depth of $9^{+\infty}/_{-4}$ km, and a length of 14 km (Figure 8). Model parameter errors (Figure 9) are 99.99% confidence intervals determined by the range of parameters within the group of models with a $\Delta\chi^2$ less than 25.7, where $\Delta\chi^2$ for a given model i is [*Press et al.*, 1992]

$$\Delta\chi = \chi_i^2 - \chi_{\text{best}}^2.$$

Figure 8 shows the best and worst fitting folds within the 99.99% confidence interval.

[21] Changes in one model parameter are compensated by changes in another parameter. This effect increases the uncertainty with which model parameters are resolvable. Figure 9a shows the trade-off in best fit displacement with changes in fault dip. Decreasing dip requires an increase in reverse displacement to achieve an acceptable fit. This is because at lower dips, less displacement goes into generating vertical uplift. Figure 9d shows the trade-off between best fit displacement and upper fault tip depth. If the upper fault tip is deeper, more displacement on the fault is required to achieve a fold of the same amplitude. Because of these trade-offs and the lack of well data on the south flank of the Hualde dome, the model places only weak constraint on the fault dip.

[22] The maximum lower fault tip depth limit cannot be estimated. Grid searches deeper than 16 km for the lower fault tip depth do not produce appreciable changes in the fold shape at the wavelength of the Coyote Hills fold (Figure 7).

[23] Figure 10a shows a north-south cross section across the Hualde dome redrawn from Figure 4b with the best fit dislocation fault model. The upper fault tip depth, lower fault tip depth, and horizontal fault location are within the errors of the best fit dislocation model. Having the thrust fault cut the upper Repetto (UR) is consistent with abrupt thickness changes within the upper and middle-lower Repetto (MR, LR) on the south flank of the Hualde dome that were shown as stratigraphic thickening unaccompanied by faulting in Figure 4b. The fault dip is consistent with fault plane reflections shown as structure contours in Figure 2 of *Shaw and Shearer* [1999; J. H. Shaw, personal communication, 2001]. The fault geometry is not consistent with a fold scarp south of the West Coyote and Hualde folds located by *Williams et al.* [2000]. A possible explanation is that this scarp is related to the bending moment at an active axial surface, analogous to the Coyote Pass Escarpment south of the Elysian Park anticline, which *Oskin et al.* [2000] described as a "parasitic fold."

6. Validation of Modeling Procedure

[24] To validate the modeling technique, we repeated the modeling procedure on the Santa Fe Springs anticline west of the Coyote Hills (Figure 10b). Folding at Santa Fe Springs results from displacement on the blind Puente Hills thrust fault [*Shaw and Shearer*, 1999]. Figure 10b shows that, as in East Coyote, folding began during deposition of the Pico member of the Fernando formation after 2.6 Ma (Appendix A). The fault dip (25°N), and upper fault tip depth (3.5 km) are known approximately from fault plane reflections and seismicity related to the 1987 Whittier Narrows earthquake [*Shaw and Shearer*, 1999]. *Allmendinger and Shaw* [2000] estimated the displacement on the fault at ~7 km based on the trishear fold modeling method. We used the dislocation model to fit a profile of the upper Repetto-Pico boundary based on the well data in Figure 10b. Using a fault length of 11 km based on the extent of subsurface folding, the dislocation modeling method yields a best fit fault with a dip

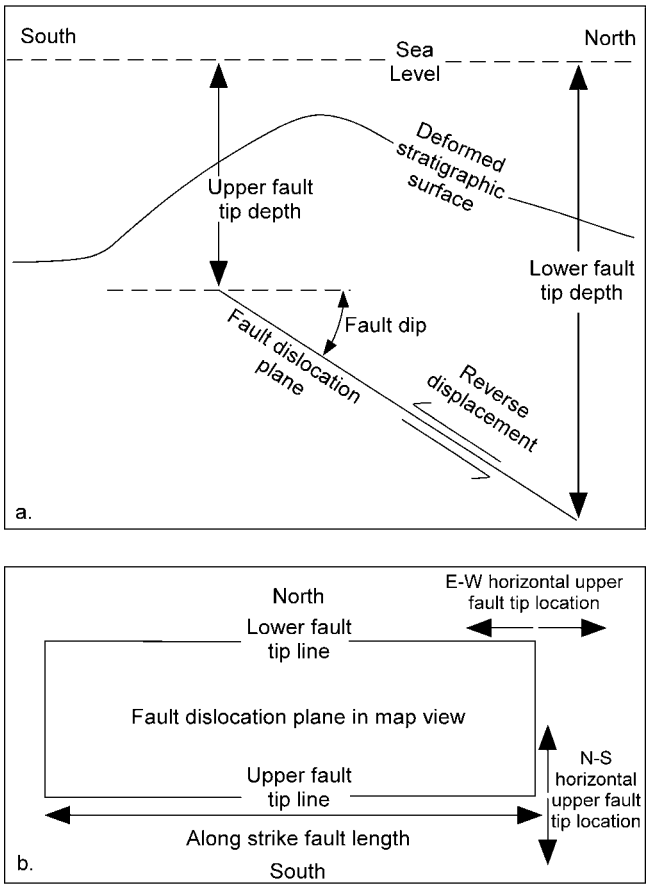

Figure 6. Dislocation model parameters. (a) Cross section view showing fault dip, upper fault tip depth, lower fault tip depth, and displacement. (b) Map projection of fault plane showing along-strike fault length, and north-south and east-west horizontal upper fault tip location.

of $15^{\circ}\,^{+40^{\circ}}/_{-10^{\circ}}$, a reverse displacement of 8 ± 3 km, an upper fault tip depth of 5.7 ± 0.7 km, a horizontal upper fault tip location of 7 ± 2 km north of well A on Figure 10b, and a lower fault tip depth of $10\,^{+\infty}/_{-1}$ km. The best fit dislocation model dip and displacement compare favorably with the dip determined from the fault plane reflections and displacement determined by trishear modeling. The dislocation model places the upper fault tip 1–3 km deeper than seismic reflection data. The deeper dislocation model upper fault tip results from assigning a constant slip along the fault plane. A dislocation model using slip that tapers off toward the upper fault tip would generate a shallower estimate of upper fault tip depth.

[25] In order to compare the fault slip between the Santa Fe Springs segment and the Coyote Hills segment of the Puente Hills thrust, we repeat the dislocation modeling for the Pico-San Pedro surface in the Santa Fe Springs Oil Field (Figure 10b). The fault dip is fixed at 25°, the upper fault tip depth at 3.5 km, and the lower fault tip depth at 13 km based on the seismic reflection results of *Shaw and Shearer* [1999]. As above, the fault length is held fixed at 11 km. The remaining parameters to fit for are fault displacement and horizontal upper fault tip location. The best fit fault has a displacement of 1800 ± 300 m and a horizontal upper fault tip location of 5.7 ± 0.1 km north of well A on Figure 10b. The modeled displacement on the Santa Fe Springs segment is consistent with the modeled slip on the Coyote Hills segment for the time period since the beginning of deposition of the San Pedro Formation.

7. Slip Rates

[26] The Pico-San Pedro contact has not been dated directly, but its age can be interpolated between two dated horizons: the Nomlaki tuff in the Santa Fe Springs Oil Field and the Brunhes-Matuyama magnetic chron boundary in a water well between the Santa Fe Springs and Montebello Oil Fields (both located on Figure 1b). An additional

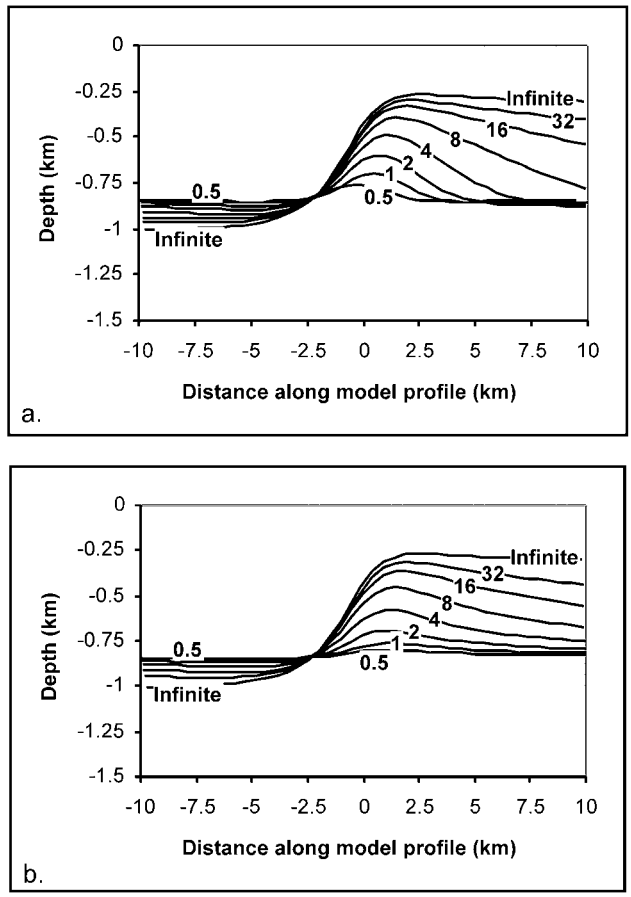

Figure 7. Response of a dislocation model to variations in (a) the depth of the lower fault tip and (b) fault length along strike to show that changing these parameters produces similar effects on fold profile amplitude and wavelength. Faults producing the folds in the above figure dip 45° in the positive *x* axis direction, have a reverse displacement of 1000 m, an upper fault tip depth of 3 km, and a horizontal upper fault tip location at 0 km along the *x* axis. The profiles are taken perpendicular to the strike of the fault and intersect the fault at its middle. The deformed surface has a depth of 0.8 km prior to folding. The *y* axis denotes depths below the surface of the model half-space. Individual profiles are labeled with depth of the lower fault tip in Figure 7a and fault length in Figure 7b, both in kilometers. The fault in Figure 7a has an infinite length and in Figure 7b has an infinite lower fault tip depth.

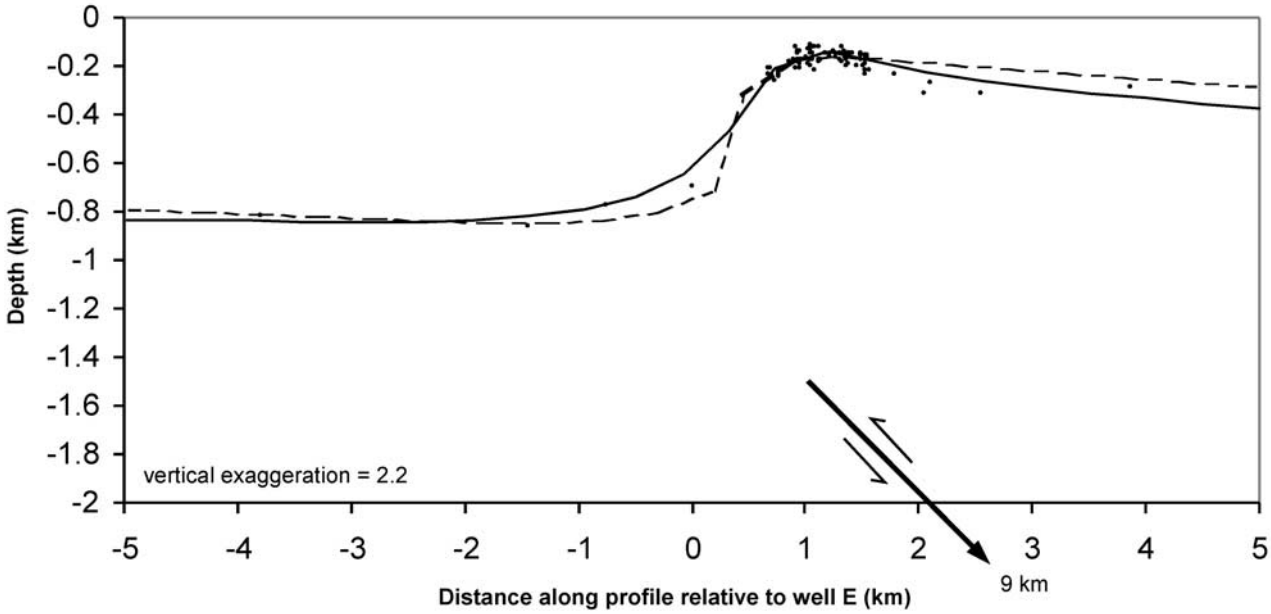

Figure 8. Geometry of best fitting fault predicted by the dislocation model for fitting the Pico-San Pedro boundary of the Hualde dome of the East Coyote Oil Field. Dots show the projection of the Pico-San Pedro boundary well control points onto a north-south plane. Curves show best fitting (solid line) and worst fitting (dashed line) fold profiles within the 99.99% confidence interval of the best fitting fault parameters. No geologic constraints are placed on the acceptability of the best fit fold profile.

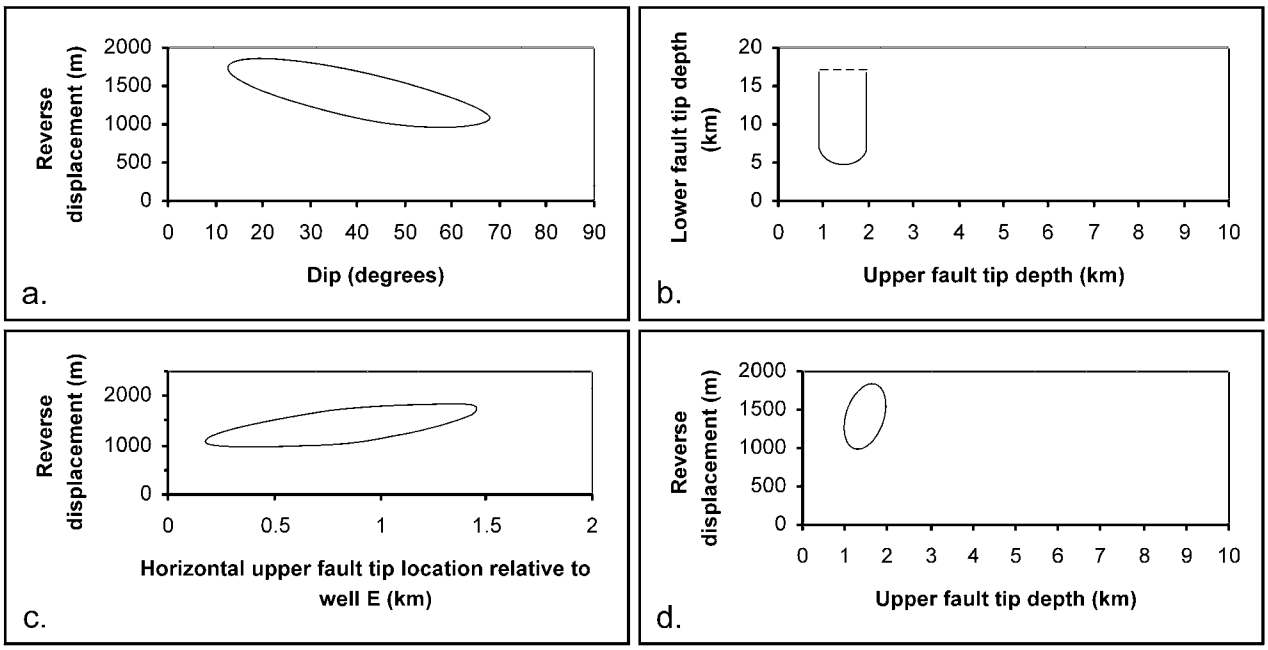

Figure 9. Confidence intervals, 99.99%, of the five-parameter space are given for the following. (a) Fault dip and reverse displacement for fitting a fault to the Pico-San Pedro boundary. (b) Upper fault tip depth and lower fault tip depth for fitting a fault to the Pico-San Pedro boundary. An upper bound on lower fault tip depth could not be found due to the reduced effect of the lower fault tip on the fold geometry as the lower fault tip deepens. The dashed line represents the maximum depth for the lower fault tip used in the dislocation models. (c) Horizontal upper fault tip location and reverse displacement for fitting a fault to the Pico-San Pedro boundary. The origin of the horizontal location axis is on Well E of Figure 4b. (d) Upper fault tip depth and reverse displacement for fitting a fault to the Pico-San Pedro boundary.

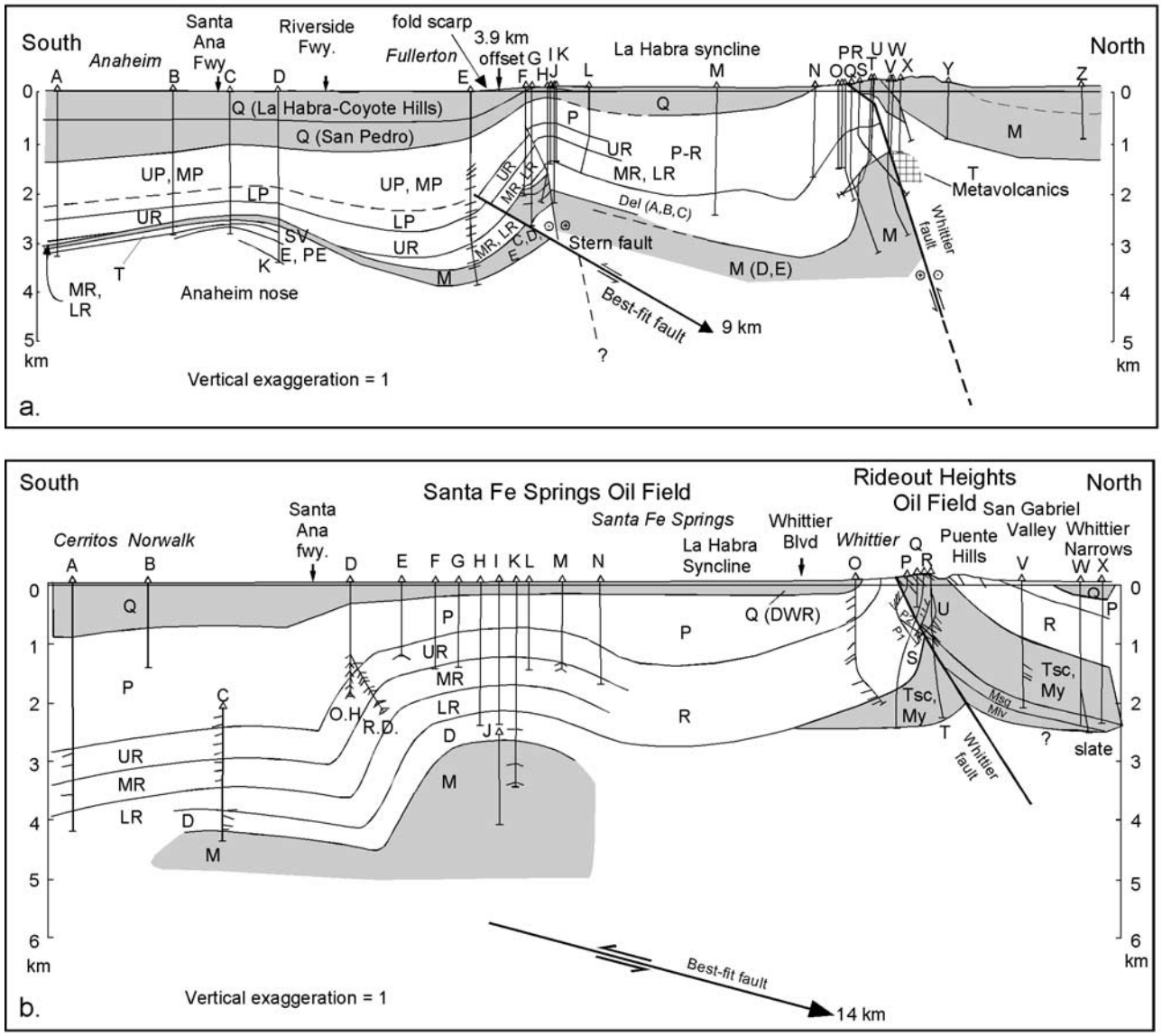

Figure 10. (a) North-south cross section redrawn from Figure 4b with a thrust fault dipping 30°N, together with the geology in the vicinity of the Whittier fault from *Bjorklund* [2002]. All fault parameters are within the errors of the best fit dislocation model and are consistent with fault plane reflections on a multichannel seismic profile [*Shaw et al.*, 2002]. Having the thrust fault cut the upper Repetto (UR) is consistent with abrupt thickness changes within the upper and middle-lower Repetto (MR, LR) on the south flank of the Hualde dome that were shown as stratigraphic thickening unaccompanied by faulting in Figure 4b. Abbreviations and symbols are the same as those in Figure 4a. (b) North-south cross section across the crest of the Santa Fe Springs anticline with best fit fault corresponding to a fold fitted to the upper Repetto-Pico boundary. See text for fault parameters. Symbols are as in Figure 4a (see also Tables B6 and B7). Additional abbreviations: O.H., original hole; R.D., redrilled hole; DWR indicates that base of San Pedro is taken from *California Department of Water Resources* [1961]; Msq, Mlv, My, older formations. Relations at Whittier fault from *Herzog* [1998].

constraint is the Sr age estimate of 1.4 ± 0.4 Ma from a mollusk in the upper San Pedro in the West Coyote Hills [*Powell and Stevens*, 2000].

[27] The Nomlaki tuff, found just above the Meyer Shale in the upper Repetto in the Union Bell 100 well in Santa Fe Springs Oil Field (A. Sarna-Wojcicki and T. H. McCulloh, personal communication, 2000), is dated by K-Ar as 3.4 ± 0.3 Ma [*Sarna-Wojcicki et al.*, 1991]. The Brunhes-Matuyama chron boundary occurs within the San Pedro Formation in the Pico Rivera water well located at 34.0014°N, 118.07673°E at a depth between 73.3 and 133.9 m, whereas the base of the San Pedro in this well is at 149.1 m. The age of this chron boundary is 780 ± 10 ka [*Spell and McDougall*, 1992]. Both the Nomlaki tuff and the Brunhes-Matuyama chron boundary were correlated to the Shell Pansini 1 oil exploratory well (well C in Figure 4e) near the water well, where they occur at 1364 ± 10 and 104 ± 30 m, respectively. Interpolating between the Nomlaki tuff and Brunhes-Matuyama chron

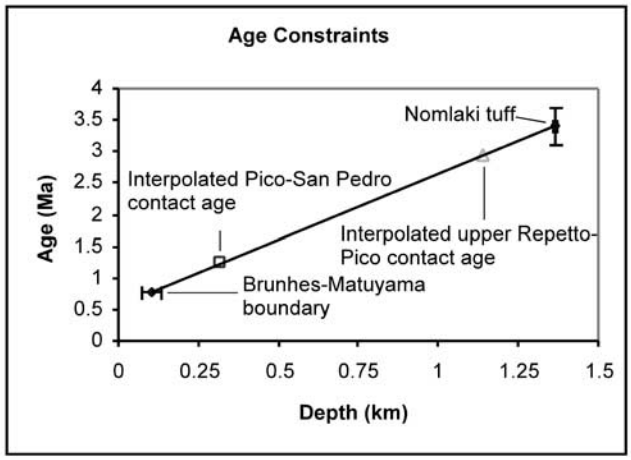

Figure 11. Age estimate of the Pico-San Pedro boundary based on interpolation between the dated Brunhes-Matuyama magnetic chron boundary and the Nomlaki tuff correlated to the Shell Pansini 1 well near the water well where the chron boundary was identified. Based on a depth of 317 m for the Pico-San Pedro contact in the Pansini well, the interpolated age of the Pico-San Pedro boundary is 1.2 ± 0.1 Ma. A depth of 1.14 km depth yields an age of 2.9 ± 0.3 Ma for the upper Repetto-Pico boundary.

boundary with the San Pedro-Pico boundary at 317 m in this well yields an age of 1.2 ± 0.1 Ma for the Pico-San Pedro boundary (Figure 11). Performing a similar calculation for the upper Repetto-Pico boundary which is at 1.14 km depth yields an age of 2.9 ± 0.3 Ma for the upper Repetto-Pico boundary.

[28] Based on the displacements calculated from the dislocation models for the Pico-San Pedro boundary, the slip rate on the blind thrust is 1.3 ± 0.5 mm/yr at the Coyote Hills and 1.5 ± 0.4 mm/yr at Santa Fe Springs for the last 1.2 Ma. Using a displacement of 8 km on the segment of the blind thrust beneath the Santa Fe Springs Oil Field from dislocation modeling of the upper Repetto-Pico boundary, we calculate an average slip rate of 3 ± 1 mm/yr for the last 2.9 Ma. These results indicate a decrease in slip rate over the last 1.2 Ma. Other workers, especially *Ponti et al.* [1996], have found a similar decrease in the growth rate of structures within the Los Angeles basin from the Pliocene to the Pleistocene. Our Coyote Hills segment slip rate agrees with recent results by *Shaw et al.* [2002] based on kinematic fault-related fold models, who calculated an average slip rate of 0.90–1.70 mm/yr for the last 1.6 Ma, with a preferred rate of 1.28 mm/yr. Our slip rate for the Santa Fe Springs segment for the last 1.2 Ma is larger than Shaw et al.'s value (0.44–0.82 mm/yr, preferred rate of 0.62 mm/yr for the last 1.6 Ma), but agrees with the average slip rate calculated by *Dolan et al.* [2003] for the last 11 ka (1.1–1.6 mm/yr) based on borehole profile across the Santa Fe Springs anticline.

8. Earthquake Magnitudes and Recurrence Intervals

[29] Knowing the slip rate and approximate geometry of the fault allows the calculation of the potential earthquake moment magnitude that could be generated by the Coyote Hills blind thrust and the recurrence interval for such an earthquake. The 1994 Northridge and 1987 Whittier Narrows earthquakes, both of which occurred on blind thrust faults in the Los Angeles Basin, had static stress drops of 100 bars [*Abercrombie and Mori*, 1994] and 155 ± 43 bars [*Lin and Stein*, 1989], respectively. A stress drop of 130 bars is assumed for the Coyote Hills blind thrust. Assuming a circular rupture on the fault, the seismic moment can be calculated from the stress drop using the equation obtained by *Keilis-Borok* [1959]

$$M_0 = \frac{16}{7} R^3 \Delta\sigma,$$

where R is the radius of rupture and $\Delta\sigma$ is the stress drop. If the model fault ruptures along its entire length of 14 km, then R = 7 km, and $M_0 = 1.0 \times 10^{19}$ N m. This yields a moment magnitude of M_w = 6.6 [*Hanks and Kanamori*, 1979]. If $\mu = 3.0 \times 10^{10}$ N m^{-2} and the expression $M_0 = \mu Ad$ [*Aki*, 1966] is solved for d, where A is the rupture area and d is the average slip on the fault during the earthquake, then d = 2.2 m. Using a slip rate of 1.3 ± 0.5 mm/yr, the recurrence interval for a M_w = 6.6 earthquake is 1700 ± 800 years.

[30] If the Coyote Hills thrust is part of the larger Puente Hills thrust system, then an earthquake might rupture both the Coyote Hills segment and the segment beneath the Santa Fe Springs Oil Field as a cascade, although this did not happen during the 1987 Whittier Narrows earthquake. In this scenario, the length of the fault becomes 26 km. Assuming a dip of 25° for the fault based on the results of *Shaw and Shearer* [1999] for the Whittier Narrows source fault and assuming that the fault ruptures to 13 km depth as it did in the 1987 Whittier Narrows earthquake, the fault would have a downdip width of 24 km. Taking R = 13 km in the above equation and using a stress drop of 130 bars yields $M_0 = 6.5 \times 10^{19}$ N m. This yields M_w = 7.2, d = 4.1 m, and an average recurrence interval of 3200 ± 1500 years using a slip rate of 1.3 ± 0.5 mm/yr. The estimated 6.6 magnitude for an earthquake on the Coyote Hills segment agrees with the value estimated by *Shaw et al.* [2002], but our recurrence intervals are approximately twice as large. This is because our estimate of rupture area during a magnitude 6.6 earthquake on the Coyote Hills segment is half of the area used by Shaw et al. Our recurrence and magnitude estimates for a cascading earthquake across the Coyote Hills and Santa Fe Springs segments agree much more closely. Shaw et al. estimated an earthquake of M_w of 7.1 every 780–2600 years, while *Dolan et al.* [2003] estimated four earthquakes with M_w 7.2–7.5 during the last 11 ka (average recurrence interval of 2800 years).

9. Discussion

9.1. Relation of Coyote Hills to Other Structures in Northeastern Los Angeles Basin

[31] *Shaw and Shearer* [1999] suggested that a system of thrust faults underlies the Puente Hills and the northern Los Angeles Basin based on oil industry seismic data. The Santa Fe Springs segment of the Puente Hills thrust fault,

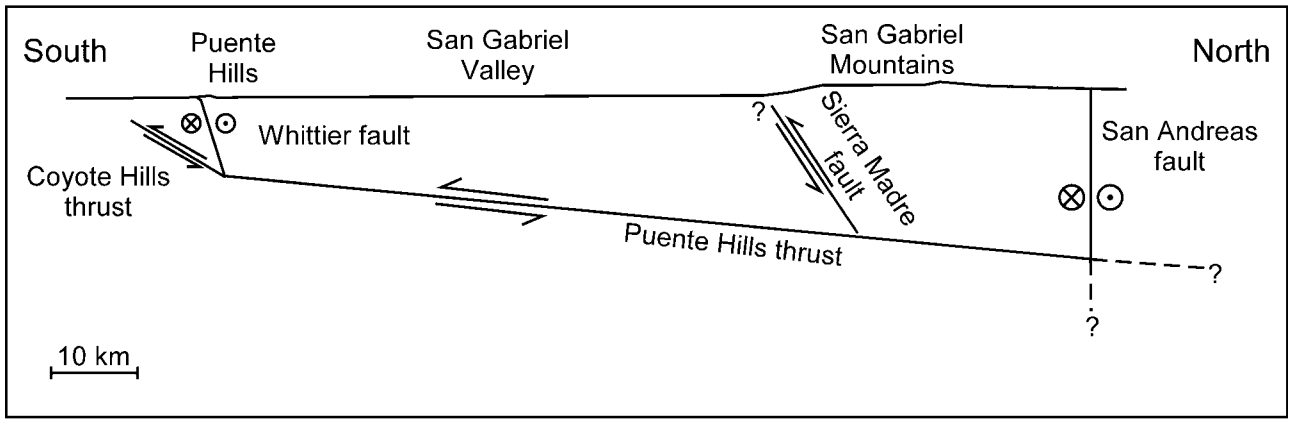

Figure 12. Schematic cross section showing the relation of the Coyote Hills thrust to the Whittier fault, the Puente Hills blind thrust, the Sierra Madre fault, and the San Andreas fault. The Whittier fault is projected to its point of intersection with the thrust fault beneath the Coyote Hills at approximately 8 km depth. This value is similar to the 10 km depth of intersection obtained for the intersection between the Whittier fault and the Puente Hills thrust based on deep seismic profile, LARSE 1 [*Fuis et al.*, 2001] suggesting that the Puente Hills thrust and the thrust beneath the Coyote Hills are part of the same thrust system.

constrained by fault plane reflections on a seismic profile and location of the main shock and aftershocks of the 1987 Whittier Narrows earthquake, dips 25°N with an upper fault tip depth of 3.5 km [*Shaw and Shearer*, 1999]. The Santa Fe Springs segment is bounded on the east by the Coyote Hills segment and on the west by the Los Angeles segment; both are en echelon, stepped right. The step over between Santa Fe Springs and West Coyote might have been the source of the Whittier earthquake of 8 July 1929, in which the isoseismal boundaries between intensities VI and VII and between VII and VIII were oriented north-south [*Richter*, 1958, pp. 37–45]. The slip rate on the Elysian Park anticline, above the Los Angeles segment, is 0.8–2.2 mm/yr, and the contraction rate is 0.6–1.1 mm/yr [*Oskin et al.*, 2000], consistent with our slip rate and convergence rate. The Coyote Hills blind thrust would intersect the right-lateral strike-slip Whittier fault at about 8 km depth, consistent with the estimated 10 km depth of this intersection based on LARSE 1 data [*Fuis et al.*, 2001]. This may be the updip part of a décollement that continues northward to the San Andreas fault [*Fuis et al.*, 2001] (Figure 12).

[32] The presence of the La Habra syncline between the Coyote Hills and Puente Hills indicates that uplift of the Puente Hills is controlled by more than just the Puente Hills blind thrust. Uplift of the footwall of the Whittier fault [*Herzog*, 1998] from Whittier to Yorba Linda, shown in Figure 10a, may be due to footwall folding in a restraining bend. Because the strike-slip rate of the Whittier fault is more than 2 mm/yr (see below), this implies slip partitioning between reverse slip on the Puente Hills blind thrust and strike slip on the Whittier fault.

[33] Slip partitioning may explain the pattern of coseismic uplift during the 1987 Whittier Narrows earthquake. *Lin and Stein* [1989] showed that uplift centered on the La Habra syncline and included both the Santa Fe Springs and the Montebello anticlines, in contrast to the late Quaternary geology. The Montebello anticline and the La Habra syncline directly to the south may deform separately due to strike slip along the Whittier fault being consumed by folding and blind thrusting at the Montebello anticline.

9.2. Transfer of Strike Slip From the Elsinore Fault to the Puente Hills and Vicinity

[34] The Elsinore fault has a late Pleistocene to Holocene strike-slip rate of 5.3–5.9 mm/yr at Glen Ivy Marsh south of Corona [*Millman and Rockwell*, 1986], with evidence for four to five earthquakes of M 6–7 since about 1060 A.D. [*Rockwell et al.*, 1986]. Northwest of Glen Ivy, the fault divides into two subparallel strands, with the northeastern strand becoming the Chino fault and the southwestern strand, following the northeastern range front of the Santa Ana Mountains, changing strike to become the Whittier fault. At Santa Ana Canyon, the Whittier fault has a right-lateral strike-slip rate of 2–3 mm/yr based on a 400 m offset of the Santa Ana River terraces that are 140 ka in age [*Gath*, 1997; *Gath et al.*, 1988; *Rockwell et al.*, 1992]. Farther west, at Olinda Creek, one strand of the Whittier fault has a right-lateral strike-slip rate of about 1 mm/yr. The stream offset by this strand is offset the same amount by another strand, and *Gath et al.* [1992] assigned a strike-slip rate on both strands of at least 2 mm/yr. The displacement is mainly by strike slip [*Gath et al.*, 1992].

[35] What accounts for the decrease of slip rate between the Elsinore and Whittier faults? The shortening rate on the Puente Hills blind thrust may account for part of the difference. The Coyote Hills anticlines are succeeded eastward by the Richfield and Kraemer anticlines, which join the Whittier fault and take up some of the slip rate. *Gath and Grant* [2002] suggest that some displacement may be taken up by uplift of the northern Santa Ana Mountains. Finally, the Chino fault takes up some of the difference. The Chino fault has tectonic expression as an oblique, right-lateral reverse fault based on northeast facing fault scarps, deflected and beheaded drainage, and vegetated lineaments

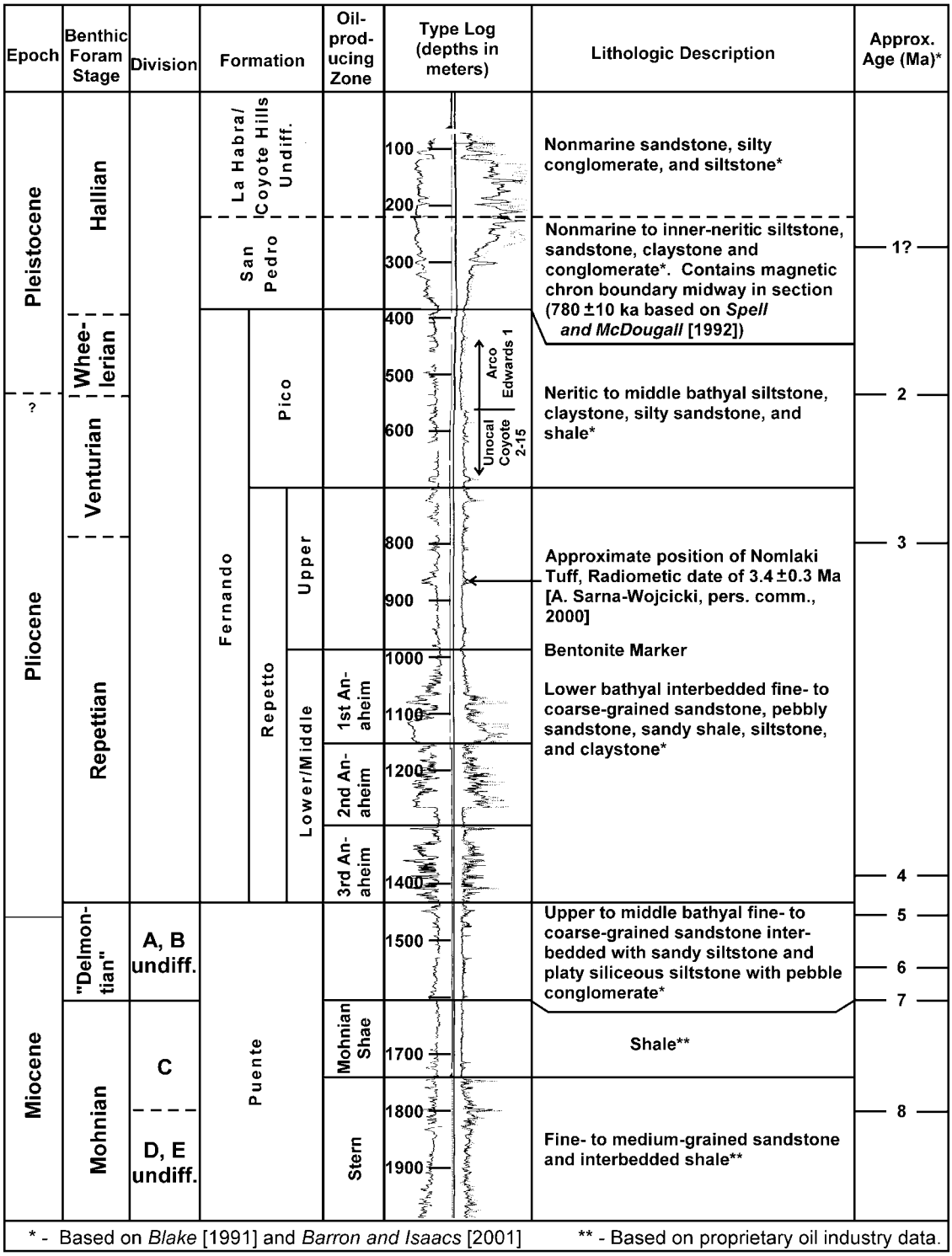

Figure A1. Type electric log and stratigraphy of East Coyote Oil Field based on the Arco Edwards 1 (shallower than 566m) and Unocal Coyote 2–15 Wells (566–1988m). See text for discussion of Pliocene and Quaternary stratigraphic units.

in alluvium. Trench excavations described by *Walls and Gath* [2001] and discussed by *Treiman* [2002] show that the Chino fault sustained 4.2–5.6 m of right-lateral strike slip from two or more events in the last 11,550 years, a slip rate of 0.36–0.51 mm/yr.

[36] Recent GPS results by *Bawden et al.* [2001] indicate that the Los Angeles basin is undergoing contraction oriented N36° ± 5°E at a rate of 4.4 ± 0.8 mm/yr. Given the east-west strike of the Puente Hills thrust system, the north-south component of contraction is approximately 3.6 mm/yr. The 1.2 ± 0.5 mm/yr north-south contraction rate calculated on the segments of the Puente thrust fault beneath the Santa Fe Springs and Coyote Oil Fields indicate that the Puente Hills thrust accommodates approximately

Table B1. List of Wells on Cross Section in Figure 4a

Well Letter	Well Name	Latitude (North)	Longitude (West)	Section-Township-Range
A	Occidental Ehrle 1	33.85111	117.88891	2-4S-10W
B	Royalty Service H-B 1	33.86291	117.88151	36-3S-10W
C	Rheem Placentia Fruit Co. 1	33.88018	117.87823	25-3S-10W
D	Utility Pet. Co. Strain 1	33.89720	117.87632	24-3S-10W
E	S. W. Bradford Smith 1	33.90088	117.87479	24-3S-10W
F	Unocal Gilman 1	33.90305	117.87621	24-3S-10W
G	Unocal Anaheim Union Water 12	33.90384	117.87663	13-3S-10W
H	Unocal Anaheim Union Water 2	33.90453	117.87721	13-3S-10W
I	Unocal Anaheim Union Water 3	33.90582	117.87752	13-3S-10W
J	Unocal Anaheim Union Water 8	33.90649	117.87748	13-3S-10W
K	Unocal Anaheim Union Water 5	33.90721	117.87745	13-3S-10W
L	Unocal Anaheim Union Water 7	33.90864	117.87758	13-3S-10W
M	Unocal Graham-Loftus 61-12	33.92514	117.87227	12-3S-10W

one third of the north-south contraction across the basin. The rest must be taken up by other structures within and at the margins of the basin.

9.3. Modeling of Geologic Structures

[37] It is somewhat surprising that our best fit fault results for the Santa Fe Springs anticline match so well with existing seismic reflection and well data [*Shaw and Shearer*, 1999] when the dislocation model neglects so many factors (fault tip propagation, tapering of displacement toward upper fault tip, evaluating fit based on a single fold profile). Furthermore, why would the dislocation model produce similar results to those from trishear modeling [*Allmendinger and Shaw*, 2000]? In the case of the Puente Hills thrust, two-dimensional trishear modeling and our pseudo-three-dimensional approach benefit from the length of the Puente Hills thrust, which places the lateral fault tips far from the location of the fold profiles. These methods would probably not work as well for a fault less than 10 km long (Figure 7). The reason for kinematic and dislocation modeling producing similar results that approximate real folds so accurately is that, to a first order, folding is largely independent of mechanical parameters such as Young's modulus and Poisson's ratio. Folding is essentially a geometric process, which only requires keeping track of the displacement of material. While a large, finite displacement on an untapered dislocation would produce physically unrealistic stresses in the medium, it reproduces observed folding well.

[38] The dislocation modeling results would have benefited from having more data along the flanks of the folds. This would allow full three-dimensional, simultaneous modeling of faults underneath the Santa Fe Springs, West Coyote, and East Coyote anticlines. This would help

Table B2. List of Wells on Cross Section in Figure 4b

Well Letter	Well Name	Latitude (North)	Longitude (West)	Section-Township-Range
A	Chevron Kellogg 1, orig. hole	33.81503	117.95564	20-4S-10W
B	Amerada Anaheim Community 48	33.83350	117.94984	8-4S-10W
C	Texaco Anaheim Community A13-1	33.84308	117.95265	8-4S-10W
D	Conoco Anaheim Community 4-1	33.84973	117.94717	5-4S-10W
E	Quinn Hiltscher 1	33.88304	117.94920	29-3S-10W
F	Unocal Hole 63	33.89311	117.90871	23-3S-10W
G	Unocal Hole 61	33.89342	117.90571	22-3S-10W
H	Unocal Hole 65	33.89620	117.90553	23-3S-10W
I	Unocal Hole 45	33.89630	117.90536	23-3S-10W
J	Unocal Hole 23	33.89718	117.90531	23-3S-10W
K	Unocal Hole 21	33.89759	117.90529	23-3S-10W
L	M. A. Cox Arroues 1	33.90331	117.90687	15-3S-10W
M	Hamilton and Sherman Union-Stewart Fee 54-10	33.92541	117.91440	10-3S-10W
N	Seacoast Wardman Community 1	33.94284	117.91030	2-3S-10W

Table B3. List of Wells on Cross Section in Figure 4c

Well Letter	Well Name	Latitude (North)	Longitude (West)	Section-Township-Range
A	Mobil Heath 2	33.86829	118.01508	34-3S-11W
B	Mobil Heath 1	33.87296	118.01148	34-3S-11W
C	Chevron Pacific Community 1	33.87520	118.00574	26-3S-11W
D	General Exploration Emery 1	33.89299	117.98361	24-3S-11W
E	General Exploration Emery-McNally 1	33.90357	117.98399	24-3S-11W
F	Derby Butch 1	33.89909	117.98135	24-3S-11W
G	Chevron Emery 98	33.89979	117.98170	24-3S-11W
H	Chevron Emery 114	33.90079	117.98170	24-3S-11W
I	Chevron Emery 112	33.90209	117.98140	24-3S-11W
J	Chevron Emery 87	33.90479	117.98070	13-3S-11W
K	Chevron Murphy Coyote 373	33.90789	117.97370	13-3S-11W
L	Chevron Emery 100	33.90857	117.98305	13-3S-11W
M	Union Stern 1	33.92042	117.98162	12-3S-11W
N	Branch Hilo Cinnabar 1	33.93667	117.97965	1-3S-11W
O	Dewey Livingston 1	33.93956	117.98080	1-3S-11W

Table B4. List of Wells on Cross Section in Figure 4d

Well Letter	Well Name	Latitude (North)	Longitude (West)	Section-Township-Range
A	California Western Koolhaas 1	33.87954	118.05879	29-3S-11W
B	Texaco Clanton 1	33.88563	118.04199	27-3S-11W
C	Mobil Librown 1	33.89074	118.02939	21-3S-11W
D	Texaco McNally 1-36	33.89271	118.02272	22-3S-11W
E	Texaco McNally A-1	33.89621	118.02267	22-3S-11W
F	Mobil McNally 1	33.89847	118.01839	15-3S-11W
G	Chevron German Community 1	33.91909	118.00483	11-3S-11W
H	Pyramid K1	33.92219	118.00112	11-3S-11W
I	Pyramid (Hathaway) Woodward 2	33.92642	117.99787	11-3S-11W
J	Rothschild Woodward 1	33.92855	117.99860	11-3S-11W
K	Rothschild Fouquet 1	33.92987	118.00145	11-3S-11W
L	Santa Fe East Whittier Community 4-1	33.94486	117.99976	2-2S-11W

Table B5. List of Wells on Cross Section in Figure 4e

Well Letter	Well Name	Latitude (North)	Longitude (West)	Section-Township-Range
A	Chevron-Otto Community 1	33.95540	118.11435	35-2S-12W
B	Hathaway-Rossi 1	33.97718	118.12071	22-2S-12W
C	Shell-Pansini 1	33.98674	118.11538	23-2S-12W
D	Empire Drilling 1	33.99475	118.10712	14-2S-12W
E	ARCO Flood Control 1	33.99549	118.10431	14-2S-12W
F	Br. American-Pico 1	34.00435	118.08961	13-2S-12W
G	Whittier Narrows-Beverly Rd. Op. Unit 1	34.01225	118.08968	12-2S-12W
H	Chevron-Scott Inv. 1	34.02444	118.08645	1-2S-12W
I	Chevron-Baldwin 110	34.02866	118.08154	1-2S-12W
J	Chevron-Baldwin 72	34.03041	118.08163	1-2S-12W

confirm whether the Puente Hills thrust is segmented between the anticlines or has a smooth surface [*Shaw et al.*, 2002]. The presence or absence of segmentation of the Puente Hills thrust has important implications for earthquake hazards within the Los Angeles Basin.

[39] Our cross sections (Figure 10) and slip rates (see above) for Santa Fe Springs and the Coyote Hills raise additional questions. The cross sections show less relief on the Pico-San Pedro boundary at Santa Fe Springs than at the Hualde dome of East Coyote. Furthermore, there is much less topographic expression of the Santa Fe Springs anticline as compared to the Coyote Hills, suggesting a reduction in Quaternary slip rate on the Puente Hills thrust from the Coyote segment to the Santa Fe Springs segment as found by *Shaw et al.* [2002]. Our Quaternary slip rate for the Santa Fe Springs segment, however, is similar to our slip rate on the Coyote Hills segment for the same time period and agrees with the Holocene slip rate of *Dolan et al.* [2003]. Resolving this conflict requires additional research into the relationships among fold growth, erosion, and deposition above the Puente Hills thrust. Geodetic data could help resolve the question, but recent geodetic results have found 5–9 mm/yr uplift rates at Santa Fe Springs that are higher than the geologic uplift rates, even when fluid injection in the oil field is taken into account [*Bawden et al.*, 2001]. The dislocation slip-rate calculations and Santa Fe Springs cross section also indicate a decrease in fault slip-rate and fold growth over the last 2.9 Ma. Confirmation of the short-term deformation rate above the Puente Hills thrust using geodetic and geomorphic data would help confirm the decrease in fold growth from East Coyote to Santa Fe Springs and would address whether the decrease in fault slip rate over time continues into the present.

Table B6. List of Wells on Cross Section in Figure 10a (Wells North of Figure 4b)

Well Letter	Well Name	Latitude (North)	Longitude (West)	Section-Township-Range
O	Cal. Resources Puente B-5	33.94649	117.90724	34-2S-10W
P	Cal. Resources Puente B-14	33.94718	117.90763	34-2S-10W
Q	Cal. Resources Puente B-9	33.94730	117.90750	34-2S-10W
R	Cal. Resources Puente B-7	33.94809	117.90544	34-2S-10W
S	Cal. Resources Puente B-8	33.94893	117.90462	34-2S-10W
T	Cal. Resources Puente B-28	33.95202	117.90512	34-2S-10W
U	Cal. Resources Puente B-32	33.95190	117.90629	34-2S-10W
V	Rowland Puente A-3	33.95403	117.90232	35-2S-10W
W	Cal. Resources Puente A3	33.95517	117.90519	34-2S-10W
X	Cal. Resources Puente A6	33.95680	117.90421	34-2S-10W
Y	Shell Puente C.H. 2	33.96645	117.90731	27-2S-10W
Z	N.O. Shively 1	33.99587	117.89506	23-2S-10W

Appendix A

[40] In Figure A1, the left curve is spontaneous potential; the right curve is resistivity. Strata shown in the type log overlay the Topanga Group (Division F of *Wissler* [1958]), older than 13.6 Ma according to the microfossil correlations of *Barron and Isaacs* [2001] and *Blake* [1991]. The Topanga Group is overlain by siltstone and sandstone of the Puente Formation, dated as 13.6 to 5.1 Ma by *Barron and Isaacs* [2001] and *Blake* [1991]. The Puente Formation is subdivided according to its microfossils into Divisions A through E by *Wissler* [1958], and ''Delmontian'' and Mohnian by *Kleinpell* [1938]. The ''Delmontian'' is referred to here in quotes because it is not the same age as the Delmontian of Kleinpell at its type locality in the central Coast Ranges [*Blake*, 1991, p. 150]. The Pliocene and Pleistocene stages (Repettian, Venturian, Wheelerian, and

Table B7. List of Wells on Cross Section in Figure 10b

Well Letter	Well Name	Latitude (North)	Longitude (West)	Section-Township-Range
A	Abraham Bloomfield Comm. 1	33.88105	118.06817	30-3S-11W
B	Farmers & Merchants 1-A	33.89145	118.06919	19-3S-11W
C	Cities Service Norwalk 1A	33.90401	118.06891	18-3S-11W
D	Mobil Comm. 14-1	33.92165	118.07977	7-3S-11W
E	Chevron Woodhead 1	33.92842	118.07559	7-3S-11W
F	Hathaway Booth 1	33.93340	118.07375	6-3S-11W
G	Chevron Koontz 13	33.93565	118.07045	6-3S-11W
H	Mobil Steinly 316-C	33.93754	118.06904	6-3S-11W
I	Texaco Weaver 364-P	33.94140	118.06732	6-3S-11W
J	Unocal Bell 107 (428-F)	33.94527	118.06642	6-3S-11W
K	Unocal Bell 100	33.94359	118.06640	6-3S-11W
L	Unocal Bell 9	33.94453	118.06331	6-3S-11W
M	Unocal W-806-C	33.94780	118.05888	32-2S-11W
N	Unocal St. Anthony Mary Barley 1	33.95343	118.05619	32-2S-11W
O	American Petrofina Whittier CH 3	33.99117	118.05348	17-2S-11W
P1	Venoco 17	33.99431	118.04215	17-2S-11W
P2	Venoco 17 rd. 3	33.99431	118.04215	17-2S-11W
Q	Seward Rideout 2	33.99813	118.04894	17-2S-11W
R	Aeco Comm. 1	34.00185	118.05180	17-2S-11W
S	Venoco 22, rd. 1	34.00330	118.05095	17-2S-11W
T	Venoco 21	34.00330	118.05097	17-2S-11W
U	Venoco 19	34.00327	118.05100	17-2S-11W
V	Premier Carla 1	34.01476	118.04829	8-2S-11W
W	Shell Bartolo 1-1	34.02360	118.04762	5-2S-11W
X	Texaco City of Whittier 1	34.02732	118.05343	5-2S-11W

Hallian) are those of *Natland* [1952]. Because of the time-transgressive nature of these zone boundaries within the Los Angeles Basin, their age is known only approximately.

Appendix B: Wells Used in Subsurface Cross Sections

[41] Latitudes, longitudes, and "Section-township-range" references are from the California Division of Oil, Gas, and Geothermal Resources (DOGGR) online well location database. Section-township-range is the American system of land measurement in which a section is approximately one square mile, a township is surveyed north or south, and a range is east or west of a surveyed baseline and meridian. A township is six sections by six sections in dimension. Section-township-range well references are provided to facilitate readers' efforts to obtain the well logs used in this study.

[42] **Acknowledgments.** This study was supported by Award 99HQ GR 0106 of the National Earthquake Hazards Reduction Program with additional support from the Southern California Earthquake Center (SCEC). SCEC is funded by NSF Cooperative Agreement EAR-0106924 and USGS Cooperative Agreement 02HQAG0008. The SCEC contribution for this paper is 481. Well data were provided by Unocal Corporation, especially Richard Salisbury, and the California DOGGR. Andrei Sarna-Wojcicki and Thane McCulloh provided information about the dated tuff bed in the Santa Fe Springs Oil Field, and Dan Ponti allowed us to use the magnetic stratigraphy from a water well north of Santa Fe Springs Oil Field. Well locations were obtained from maps and digital data were published by DOGGR. The geology of the Whittier fault shown in Figure 10a was provided by *Bjorklund* [2002] when his thesis was in draft form. Patrick Keeffe provided near-surface geologic data in the East Coyote Oil Field. Fieldwork by D.J.M. was facilitated by a summer intern position with Earth Consultants International. Gary Huftile assisted in obtaining well data. Pierfrancesco Burrato of the Istituto Nazionale di Geofisica constructed an early version of the West Coyote and Leffingwell cross sections shown in Figures 4c and 4d. Discussions with Eldon Gath, Tania Gonzalez, Jack Hillhouse, Dan Ponti, Chuck Powell, Tom Rockwell, Kay St. Peter, John Shaw, Siang Tan, Chris Walls, and Tom Wright added to our understanding of the problem.

References

Abercrombie, R., and J. Mori, Stress drops of the Northridge mainshock and larger aftershocks, *Seismol. Res. Lett.*, *65*, 243, 1994.

Aki, K., Generation and propagation of *G* waves from the Nigata earthquake of June 16, 1964, part 2, Estimation of earthquake moment, release energy, and stress-strain drop from the *G* wave spectrum, *Bull. Earthquake Res. Inst. Univ. Tokyo*, *44*, 73–88, 1966.

Allmendinger, R. W., and J. H. Shaw, Estimation of fault propagation distance from fold shape: Implications for earthquake hazard assessment, *Geology*, *28*, 1099–1102, 2000.

Barron, J. A., and C. M. Isaacs, Updated chronostratigraphic framework for the California Miocene, in *The Monterey Formation: From Rocks to Molecules*, edited by C. M. Isaacs and J. Rullkötter, pp. 393–395, Columbia Univ. Press, New York, 2001.

Bawden, G. W., W. Thatcher, R. S. Stein, K. W. Hudnut, and G. Peltzer, Tectonic contraction across Los Angeles after removal of groundwater pumping effects, *Nature*, *412*, 812–815, 2001.

Benedetti, L., P. Tapponnier, G. C. P. King, B. Meyer, and I. Manighetti, Growth folding and active thrusting in the Montello region, Beneto, northern Italy, *J. Geophys. Res.*, *105*, 739–766, 2000.

Bent, A. L., and D. V. Helmberger, Source complexity of the October 1, 1987, Whittier Narrows earthquake, *J. Geophys. Res.*, *94*, 9548–9556, 1989.

Bjorklund, T. K., Evolution of the Whittier fold-fault system of the northeastern Los Angeles Basin, California, Ph.D. thesis, 128 pp., Univ. of Houston, Houston, Tex., 2002.

Blake, G. H., Review of the Neogene biostratigraphy and stratigraphy of the Los Angeles Basin and implications for basin evolution, in *Active Margin Basins*, edited by K. T. Biddle, *AAPG Mem.*, *52*, 135–184, 1991.

California Department of Water Resources, Planned utilization of the groundwater basin of the coastal plain of Los Angeles County, *Bull. Calif. Dep. Water Resour.*, *104*, *Appendix A*, *Cross Section N-N'*, *Ground Water Geology*, 181 pp., 1961.

Davis, T. L., J. Namson, and R. F. Yerkes, A cross section of the Los Angeles area: Seismically active fold and thrust belt, the 1987 Whittier Narrows earthquake, and earthquake hazard, *J. Geophys. Res.*, *94*, 9644–9664, 1989.

Dibblee, T. W., Jr., Geologic map of the Whittier and La Habra quadrangles (western Puente Hills), Los Angeles and Orange counties, California, *Map 74*, scale 1:24,000, Dibblee Geol. Found., Camarillo, Calif., 2001a.

Dibblee, T. W., Jr., Geologic map of the Yorba Linda and Prado Dam quadrangles (eastern Puente Hills), Los Angeles, Orange, San Bernardino, and Riverside counties, California, *Map 75*, scale 1:24,000, Dibblee Geol. Found., Camarillo, Calif., 2001b.

California Division of Oil, Gas, and Geothermal Resources, Santa Fe Springs, *Map 102*, Sacramento, Calif., 1997a.

California Division of Oil, Gas, and Geothermal Resources, Montebello, *Map 103*, Sacramento, Calif., 1997b.

California Division of Oil, Gas, and Geothermal Resources, Whittier-Sansinena, *Map 104*, Sacramento, Calif., 1997c.

California Division of Oil, Gas, and Geothermal Resources, West Coyote-Leffingwell, *Map 105*, Sacramento, Calif., 1997d.

California Division of Oil, Gas, and Geothermal Resources, Brea-Olinda-East Coyote, *Map 106*, Sacramento, Calif., 1997e.

California Division of Oil, Gas, and Geothermal Resources, Los Angeles and Orange counties, *Map W1-5*, Sacramento, Calif., 2000.

Dolan, J. F., S. A. Christofferson, and J. H. Shaw, Recognition of paleoearthquakes on the Puente Hills blind thrust fault, California, *Science*, *299*, 115–118, 2003.

Fuis, G. S., T. Ryberg, N. J. Godfrey, D. A. Okaya, and J. M. Murphy, Crustal structure and tectonics from the Los Angeles Basin to the Mojave Desert, southern California, *Geology*, *29*, 15–18, 2001.

Gath, E. M., Tectonic geomorphology of the eastern Los Angeles Basin, *U.S. Geol. Surv. Final Tech. Rep.*, *NEHRP grant 1431-95-G-2526*, 13 pp., 1997.

Gath, E. M., and L. B. Grant, Is the Elsinore fault responsible for the uplift of the Santa Ana Mountains, Orange county, California?, *Geol. Soc. Am. Abstr. Programs*, *24*, 5, 2002.

Gath, E. M., J. H. Hanson, B. R. Clark, and T. K. Rockwell, The Whittier fault in southern California: Preliminary results of investigations, *EOS Trans. AGU*, *69*, 260, 1988.

Gath, E. M., T. Gonzalez, and T. K. Rockwell, Slip rate of the Whittier fault based on 3-D trenching at Brea, southern California, *Geol. Soc. Am. Abstr. Programs*, *24*, 26, 1992.

Gray, C. H., Geology of the Corona South Quadrangle and the Santa Ana Narrows area, Riverside, Orange, and San Bernardino counties, California, *Bull. Calif. Div. Mines Geol.*, *178*, 5–58, 1961.

Hanks, T. C., and H. Kanamori, A moment-magnitude scale, *J. Geophys. Res.*, *84*, 2348–2350, 1979.

Hauksson, E., and L. M. Jones, The 1987 Whittier Narrows earthquake sequence in Los Angeles, southern California: Seismological and tectonic analysis, *J. Geophys. Res.*, *94*, 9569–9589, 1989.

Herzog, D. W., Subsurface structural evolution along the northern Whittier fault zone of the eastern Los Angeles Basin, southern California, M. S. thesis, 53 pp., Oreg. State Univ., Corvallis, 1998.

Keilis-Borok, V. I., On the estimation of the displacement in an earthquake source and of source dimensions, *Ann. Geophys.*, *12*, 205–214, 1959.

King, G. C. P., R. S. Stein, and J. B. Rundle, The growth of geological structures by repeated earthquakes: 1. Conceptual framework, *J. Geophys. Res.*, *93*, 13,307–13,318, 1988.

King, G. C. P., R. S. Stein, and J. Lin, Static stress changes and the triggering of earthquakes, *Bull. Seismol. Soc. Am.*, *84*, 935–953, 1994.

Kleinpell, R. M., *Miocene Stratigraphy of California*, 450 pp., Am. Assoc. of Pet. Geol., Tulsa, Okla., 1938.

Lin, J., and R. S. Stein, Coseismic folding, earthquake recurrence, and the 1987 source mechanism at Whittier Narrows, Los Angeles Basin, California, *J. Geophys. Res.*, *94*, 9614–9632, 1989.

Millman, D. E., and T. K. Rockwell, Neotectonics of the Elsinore fault in Temescal Valley, California, in *Neotectonics and Faulting in Southern California*, volume and guidebook, pp. 159–166, Geol. Soc. of Am., Cordilleran Sect., Boulder, Colo., 1986.

Myers, D., Structural geology and dislocation modeling of the East Coyote anticline, eastern Los Angeles basin, M. S. thesis, 54 pp., Oreg. State Univ., Corvallis, 2001.

Natland, M. L., Pleistocene and Pliocene stratigraphy of southern California, Ph.D. dissertation, 350 pp., Univ. of Calif., Los Angeles, 1952.

Okada, Y., Internal deformation due to shear and tensile faults in a half-space, *Bull. Seismol. Soc. Am.*, *82*, 1018–1040, 1992.

Oskin, M., K. Sieh, T. Rockwell, G. Miller, P. Guptill, M. Curtis, S. McArdle, and P. Elliot, Active parasitic folds on the Elysian Park anticline: Implica-

tions for seismic hazard in central Los Angeles, California, *Geol. Soc. Am. Bull.*, *112*, 693–707, 2000.

Ponti, D. J., J. P. Quinn, and J. W. Hillhouse, Quaternary chronostratigraphic constraints on deformation and blind-thrust faulting, northern Los Angeles Basin, California (abstract), *Eos Trans. AGU*, *77*(46), Fall Meet. Suppl., F644, 1996.

Powell, C. L. and D. Stevens, Age and paleoenvironmental significance of mega-invertebrates from the "San Pedro" Formation in the Coyote Hills, Fullerton and Buena Park, Orange county, southern California, *U.S. Geol. Surv. Open File Rep. 00-319*, 83 pp., 2000.

Press, W. H., B. P. Flannery, S. A. Tuekolsky, and W. T. Vetterling, *Numerical Recipes: The Art of Scientific Computing*, 2nd ed., 692 pp., Cambridge Univ. Press, New York, 1992.

Richter, C. F., *Elementary Seismology*, 768 pp., W. H. Freeman, New York, 1958.

Rockwell, T. K., R. S. McElwain, D. E. Millman, and D. L. Lamar, Recurrent late Holocene faulting on the Glen Ivy North strand of the Elsinore fault at Glen Ivy Marsh, in *Neotectonics and Faulting in Southern California*, pp. 167–175, Geol. Soc. of Am., Cordilleran Sect., Boulder, Colo., 1986.

Rockwell, T. K., E. M. Gath, and T. Gonzalez, Sense and rate of slip on the Whittier fault zone eastern Los Angeles Basin, California, in *Proceedings of the 35th Annual Meeting of the Association of Engineering Geologists*, edited by M. L. Stout, p. 679, Assoc. of Eng. Geol., Santa Ana, Calif., 1992.

Sarna-Wojcicki, A. M., K. R. Lajoie, C. E. Meyer, D. P. Adam, and H. J. Rieck, Tephrochronologic correlation of upper Neogene sediments along the Pacific margin, conterminous United States, in *The Geology of North America*, vol. K2, *Quaternary Nonglacial Geology*: *Conterminous United States*, edited by R. B. Morrison, pp. 117–140, Geol. Soc. of Am., Goulder, Colo., 1991.

Schneider, C. L., C. Hummon, R. S. Yeats, and G. J. Huftile, Structural evolution of the northern Los Angeles basin, California, based on growth strata, *Tectonics*, *15*, 341–355, 1996.

Shaw, J. H., and P. M. Shearer, An elusive blind-thrust fault beneath metropolitan Los Angeles, *Science*, *283*, 1516–1518, 1999.

Shaw, J. H., and J. Suppe, Earthquake hazards of active blind thrust faults under the central Los Angeles Basin, California, *J. Geophys. Res.*, *101*, 8623–8642, 1996.

Shaw, J. H., A. Plesch, J. F. Dolan, T. L. Pratt, and P. Fiore, Puente Hills blind-thrust system, Los Angeles, California, *Bull. Seismol. Soc. Am.*, *92*, 2946–2960, 2002.

Spell, T. L., and I. McDougall, Revisions to the age of the Brunhes-Matuyama boundary and the Pleistocene geomagnetic polarity timescale, *Geophys. Res. Lett.*, *19*, 1181–1184, 1992.

Tan, S. S., R. V. Miller, and J. R. Evans, Environmental geology of parts of the La Habra, Yorba Linda and Prado Dam quadrangles, Orange county, California, *Calif. Div. Mines Geol. Open File Rep. 84-24LA*, 119 pp., 1984.

Tearpock, D. J., and R. E. Bischke, *Applied Subsurface Geological Mapping*, 648 pp., Prentice-Hall, Old Tappan, N. J., 1991.

Toda, S., R. S. Stein, P. A. Reasenberg, J. H. Dieterich, and A. Yoshida, Stress transferred by the 1995 M_w = 6.9 Kobe, Japan, shock: Effect on aftershocks and future earthquake probabilities, *J. Geophys. Res.*, *103*, 24,543–24,565, 1998.

Treiman, J. A., Chino fault, Riverside and San Bernardino counties, California, *Calif. Geol. Surv. Fault Eval. Rep. FER 247*, 18 pp., 3 plates, Calif. Geol. Surv., Los Angeles, Calif., 2002.

Walls, C., and E. M. Gath, Tectonic geomorphology and Holocene surface rupture on the Chino fault, paper presented at SCEC Annual Meeting, S. Calif. Earthquake Cent., Oxnard, Calif., 2001.

Ward, S. N., A note on the surface volume change of shallow earthquakes, *Geophys. J. R. Astron. Soc.*, *85*, 461–466, 1986.

Ward, S. N., and G. Valensise, The Palos Verdes terraces, California: Bathtub rings from a buried reverse fault, *J. Geophys. Res.*, *99*, 4485–4494, 1994.

Williams, R. A., T. L. Pratt, K. J. Odum, W. J. Stephenson, J. F. Dolan, S. Christofferson, and J. H. Shaw, High-resolution seismic imaging of active axial surfaces above the Puente Hills thrust fault, Los Angeles Basin, California, *Eos Trans. AGU*, *81*(48), Fall Meet. Suppl., Abstract S61D-03, 2000.

Wissler, S. G., Correlation chart of producing zones of Los Angeles Basin Oil Fields, in *A Guide to the Geology and Oil Fields of the Los Angeles and Ventura Regions*, edited by J. W. Higgins, pp. 59–61, Pac. Sect., Am. Assoc. of Pet. Geol., Los Angeles, Calif., 1958.

Wright, T. L., Structural geology and tectonic evolution of the Los Angeles Basin, in *Active Margin Basins*, edited by K. T. Biddle, *AAPG Mem., 52*, 35–134, 1991.

Yerkes, R. F., Geology and oil resources of the western Puente Hills area, southern California, *U.S. Geol. Surv. Prof. Pap. 420-C*, 63 pp., 1972.

Yerkes, R. F., T. H. McCulloh, J. E. Schoellhamer, and J. G. Vedder, Geology of the Los Angeles Basin, California—An introduction, *U.S. Geol. Surv. Prof. Pap. 420-A*, 57 pp., 1965.

D. J. Myers, Division of Natural Sciences and Mathematics, Western Oregon University, 345 North Monmouth Avenue, Monmouth, OR 97361, USA. (myersd@wou.edu)

J. L. Nabelek, College of Oceanic and Atmospheric Sciences, Oregon State University, Corvallis, OR 97331, USA. (nabelek@coas.oregonstate.edu)

R. S. Yeats, Department of Geosciences, Oregon State University, Corvallis, OR 97331, USA. (yeatsr@geo.orst.edu)